This paper is published as part of a PCCP Themed Issue on:

Synergies between Experimental and Theoretical Studies of Gas Phase Reactions

Guest Edited by: Paul Seakins (Leeds) and Struan Robertson (Accelrys, Cambridge and Leeds)

Published in issue 31, 2007 of PCCP

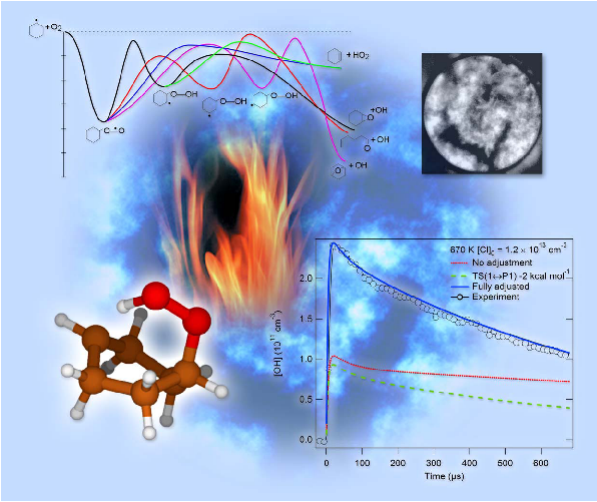

Image reproduced by permission of Dr Taatjes and Linda A.Houston for Sandia National Laboratories from *Phys.Chem.Chem.Phys.*, 2007, **9**, 4315-4331

Other papers published in this issue include:

Direct detection of polyynes formation from the reaction of ethynyl radical (C_2H) with propyne (CH_3–C≡CH) and allene (CH_2=C=CH_2)
Fabien Goulay, David L. Osborn, Craig A. Taatjes, Peng Zou, Giovanni Meloni and Stephen R. Leone, *Phys. Chem. Chem. Phys.*, 2007
DOI: 10.1039/b614502g

Master equation methods for multiple well systems: application to the 1-,2-pentyl system
Struan H. Robertson, Michael J. Pilling, Luminita C. Jitariu and Ian H. Hillier, *Phys. Chem. Chem. Phys.*, 2007
DOI: 10.1039/b704736c

***Ab initio* methods for reactive potential surfaces**
Lawrence B. Harding, Stephen J. Klippenstein and Ahren W. Jasper, *Phys. Chem. Chem. Phys.*, 2007
DOI: 10.1039/b705390h

Visit the website for both cutting edge research papers and authoritative review articles by leaders in a range of fields

www.rsc.org/pccp

Ab initio methods for reactive potential surfaces

Lawrence B. Harding,* Stephen J. Klippenstein and Ahren W. Jasper

Received 10th April 2007, Accepted 10th May 2007
First published as an Advance Article on the web 6th June 2007
DOI: 10.1039/b705390h

Case studies of ten reactions using a variety of standard electronic structure methods are presented. These case studies are used to illustrate the usefulness and shortcomings of these standard methods for various classes of reactions. Limited comparisons with experiment are made. The reactions studied include four radical–radical combinations, $H + CH_3 \rightarrow CH_4$, $CH_3 + CH_3 \rightarrow C_2H_6$, $H + HCO \rightarrow H_2CO$ and $CH_3 + HCO \rightarrow CH_3CHO$, three abstraction reactions, $H + HO_2 \rightarrow H_2 + O_2$, $H + HCO \rightarrow H_2 + CO$ and $CH_3 + HCO \rightarrow CH_4 + CO$, a radical–molecule addition, $H + HCCH \rightarrow C_2H_3$, and two molecular decompositions, $H_2CO \rightarrow H_2 + CO$ and $CH_3CHO \rightarrow CH_4 + CO$. The electronic structure methods used are DFT, MP2, CCSD(T), QCISD(T), CASSCF, CASPT2, and CAS + 1 + 2 + QC.

1. Introduction

In the past 10–15 years there has been a dramatic improvement in the accuracy of *ab initio* methods as applied to reactive potential energy surfaces.[1] This can be traced to improvements in methodology, basis sets and computer technology. As a result of these improvements, accurate, *a priori* predictions of reaction rates involving relatively small, gas phase, reactants are becoming almost routine. Increasingly, *a priori* predictions of reaction rates are being used to aid in both the interpretation and design of experimental measurements. A complete review of *ab initio* methods is beyond the scope of this paper. Instead we will present several case studies comparing results obtained with a number of popular, *ab initio* methods. The goal here is to provide the non-specialist reader with insights into when particular methods can be expected to be reliable and when they can be expected to fail.

A key factor in the accuracy of any *ab initio* calculation is the basis set. A complete review of basis set issues is beyond the scope of this article. Suffice it to say that ideally one systematically increases the size of the basis set until the results converge to within some desired limits of accuracy. The Dunning correlation consistent basis sets[2,3] are ideally suited to this purpose, although for larger systems the calculations often become intractable before the desired accuracy is achieved. This often necessitates the use of basis set corrections of various kinds, (for example, SEC,[4,5] SAC,[6,7] and CBS[8–18]) topics that are again beyond the scope of this paper.

In this paper we report studies of ten reactions using a variety of standard electronic structure methods. The reactions chosen for this study include four radical–radical addition reactions, $H + CH_3$, $CH_3 + CH_3$, $H + HCO$ and $CH_3 + HCO$, three abstraction reactions, $H + HO_2 \rightarrow H_2 + O_2$, $H + HCO \rightarrow H_2 + CO$ and $CH_3 + HCO \rightarrow CH_4 + CO$, one radical-molecule addition reaction, $H + HCCH$ and two molecular dissociations $H_2CO \rightarrow H_2 + CO$ and $CH_3CHO \rightarrow CH_4 + CO$.

Chemistry Division, Argonne National Laboratory, Argonne, IL, 60439, USA. E-mail: harding@anl.gov

In section 2 we give a brief description of the theoretical methods used. In Section 3 we report the results for the ten chosen reactions. The primary focus of these calculations is on testing the effectivness of the different electronic structure methods for predicting the kinetics of various classes of reactions. Limited comparisons with experiment are presented as an aid in examining this effectiveness. Finally in Section 4 we give some general conclusions.

2. Methodology

2.1 Quantum chemistry

In this paper we report results using up to eight different standard electronic structure methods. These include two variants of density functional theory (DFT), a number of single reference methods including Hartree–Fock (HF), second order, Møller–Plesset perturbation theory (MP2), coupled-cluster (CCSD(T)[19]), quadratic configuration interaction (QCISD(T)[20]) and a number of multi-reference methods including complete active space self-consistent field theory (CASSCF), multi-reference, second-order, perturbation theory (CASPT2[21,22]), and multi-reference, singles and doubles, configuration interaction, CAS + 1 + 2 + QC. The electronic structure calculations were done using the GAUSSIAN98[23] and MOLPRO[24] program packages.

Because there are literally hundreds of DFT methods to choose from, a complete review of DFT methods is beyond the scope of this paper (see ref. 25 for a recent study of the accuracy of a number of DFT methods). Here we simply chose two representative DFT methods, B3LYP and MPW1K. B3LYP is probably the single most widely used DFT method. Originally proposed by Becke[26] in 1993, it contains three empirical parameters, which were optimized to fit a set of experimental atomization energies, ionization energies and proton affinities. As noted by Hertwig *et al.*[27] there are at least two different implementations of B3LYP. We use the GAUSSIAN98 implementation. The MPW1K method was developed by Lynch *et al.*[28] It contains one parameter, which was optimized to reproduce the barrier heights and

energies of reaction for a set of 20 abstraction reactions using a 6-31 + G** basis set. All of the DFT calculations reported here were done using the GAUSSIAN98 program.

For the single reference methods an important distinction has to be made between spin restricted and spin unrestricted calculations. In spin restricted calculations the orbitals corresponding to the alpha and beta spin electrons are required to be the same and the resulting wavefunctions are guaranteed to be spin eigenfunctions. In spin un-restricted calculations the alpha and beta orbitals are allowed to be different and the wavefunctions are not guaranteed to be spin eigenfunctions, *i.e.* they can contain mixtures of, for example, singlet and triplet character. For Hartree–Fock calculations restricted and un-restricted calculations are abbreviated RHF and UHF, respectively and similarly RMP2 and UMP2 for second-order Møller–Plesset perturbation theory. The MP2 calculations reported here were done using the GAUSSIAN98 program.

For CCSD(T) and QCISD(T) calculations a further distinction must be made. In the GAUSSIAN98 implementation, either RHF or UHF orbitals can be used for closed shell (singlet) systems, while for open shell systems only UHF orbitals can be used. In the MOLPRO implementation[29,30] all CCSD(T) and QCISD(T) calculations use a single set of orbitals for both alpha and beta spins. For closed shell calculations then these will be the same as the GAUSSSIAN, RHF based calculations. For open shell calculations however, the MOLPRO implementation employs spin restricted, open shell HF (ROHF) orbitals while, as noted above, GAUSSIAN employs spin un-restricted, UHF orbitals. In the MOLPRO implementation even though the ROHF reference wavefunction is guaranteed to be a spin eigenfunction the open shell, CCSD(T) and QCISD(T) wavefunctions are not. MOLPRO has the option of doing the open shell CCSD(T) and QCISD(T) calculations using either a spin un-restricted or partially spin-restricted formalism. To distinguish between these variants we will use the following abbreviations:

RCCSD(T) RQCISD(T)	GAUSSIAN/MOLPRO, closed shell spin restricted
UCCSD(T) UQCISD(T)	GAUSSIAN, open shell spin un-restricted
ROHF-RCCSD(T) ROHF-RQCISD(T)	MOLPRO open shell partially spin restricted,
ROHF-UCCSD(T) ROHF-UQCISD(T)	MOLPRO open shell spin un-restricted,

Two kinds of multi-reference calculations will be employed here, CASPT2 and CAS + 1 + 2 + QC. The CASPT2 calculations use the MOLPRO implementation of Celani and Werner.[31–33] The CAS + 1 + 2 + QC configuration interaction calculations use the internally contracted implementation of Werner and Knowles[34,35] and include a multi-reference Davidson correction[36,37] for the effects of higher-order excitations. All of the multi-reference calculations were done with the MOLPRO program.

2.2 Kinetics

Quantum chemistry methods are often tested against experimental or higher-level theoretical thermochemistry . Such tests may not be particularly informative when choosing a method for kinetics. Instead, the significance of the differences in the various electronic structure results should be examined through their effect on the reaction rate coefficients. Here, we employ transition state theory (TST) as a means for estimating the rate coefficients and thus illustrating the quantitative kinetic importance of the differences. Other approaches for estimating the rate constant, such as quantum or classical dynamics, would be expected to provide similar variations with electronic structure method.

Within TST the rate coefficient is given by

$$k(T) = \kappa \frac{k_B T}{h} \frac{Q^\dagger}{Q_R} \exp(-V^\dagger / k_B T) \qquad (1)$$

where κ is the transmission coefficient, k_B is Boltzmann's constant, T is temperature, h is Planck's constant, $V^\dagger$ is the electronic (classical) barrier height, Q_R is the total partition function for reactants, and $Q^\dagger$ is the partition function for motion on the transition state dividing surface. The transition state is defined as the dividing surface that provides the best separation between reactants and products, and is obtained by minimizing the calculated partition function as a function of a reaction coordinate s.

The exponential dependence of the rate constant on the barrier height implies that, at least near room temperature, the primary difference between alternative electronic structure methods is with regard to their predictions for $V^\dagger$. Even a small error in the barrier height (*e.g.*, less than 0.5 kcal mol^{-1}) can have a significant effect on the computed rate coefficient at room temperature.

At higher temperatures (*e.g.*, above 1000 K), the Boltzmann factor is closer to unity and uncertainties in the predicted partition functions become more significant than uncertainties in the barrier height. In typical applications of eqn (1), the partition functions for the transition state and the reactants are treated within the harmonic oscillator and rigid rotor approximations, and so these quantities are functions of the harmonic frequencies obtained from the local second derivatives of the potential energy surface. (These partition functions are also proportional to the rotational constants, but the structural differences for alternative electronic structure methods tend to yield only minor variations in the rotational constants.) At high temperatures, the term $Q^\dagger/Q_R$ becomes proportional to the ratio of vibrational frequencies for the reactants and the transition state. Notably, the predicted vibrational frequencies, and thus rate coefficients, can depend quite strongly on the electronic structure method. This dependence is due at least in part to the variations in the predicted geometry for the transition state.

The transmission coefficient κ is a number greater than unity that models the effect of tunneling through the reaction barrier. For reactions involving H atom motions, variations

This journal is © the Owner Societies 2007

in the predicted transmission coefficient are important, particularly at low temperature. In the small curvature tunneling (SCT) of Truhlar *et al.*[38] κ is obtained by integrating the semiclassical action along the reaction path for several total energies and scaling the effective mass to account for tunneling paths that deviate from the reaction path. In this approximation, κ is sensitive to the width of the barrier near the saddle point (or, more precisely, to the width of the vibrationally adiabatic ground state energy along the reaction path). Tunneling decreases rapidly with temperature, and errors in κ are expected to affect the accuracy of the rate calculations most significantly at low temperatures. More sophisticated treatments of tunneling are available[39,40] but are beyond the scope of this paper.

The effects on the computed rate coefficient of errors in the barrier height and in the barrier width, while often significant individually, typically have opposite effects, such that an improvement in the description of only one aspect may, in fact, result in a less accurate prediction for the overall rate coefficient. Furthermore, it is often convenient to use different levels of theory to characterize different aspects of the potential energy surface. For example, low-level methods may be necessary for determining optimized structures and frequencies due to the relatively high cost of evaluating the Hessian, whereas energies at particular stationary points are often computed at much higher levels of theory. Thus, it will be worthwhile to also consider the changes in various components of the calculations.

The present applications of TST to reactions with a well defined barrier are based on rigid-rotor harmonic-oscillator assumptions. In each case, we consider a fixed transition state at the location of the electronic saddle point. Variational optimizations of the transition state location are not considered here, partly because they are expected to have only a modest effect on the rate predictions. Furthermore, our interest is in studying the dependence on the electronic structure methods, rather than on obtaining highly accurate rate predictions. Thus, we also do not consider anharmonic effects. For the H + C_2H_2 reaction and the tight transition state for H_2CO decomposition, tunneling is treated as occurring through an asymmetric Eckart potential. For the H + HO_2 reaction, we implement the small curvature tunneling approximation and also consider the variation of the electronic saddlepoint away from the low level saddlepoint when considering the coupled high level/low level calculations. For the latter reaction, we used the POLYRATE[41] kinetics package and the GAUSSRATE[42] interface (in a modified form with MOLPRO electronic structure evaluations for the CASPT2 reaction paths).

For barrierless reactions, as in the present radical–radical channels, the transition state location is highly variable, and a qualitatively accurate treatment must consider the anharmonicities and couplings for the interfragment modes. The variable reaction coordinate transition state theory approach[43–45] provides an accurate and yet efficient means for treating such reactions. Here we implement this approach with direct evaluations of the interaction energies, which greatly simplifies the evaluations for multiple electronic structure methods. The orientational integrations are converged to about 5% and the variational minimizations are performed at the energy E and total angular momentum J resolved level. A limited number of dividing surfaces are considered, consisting of a set of center-of-mass separation distance based surfaces at long-range and partially optimized radical orbital based dividing surfaces at short range. More complete dividing surface optimizations might yield reductions in the rate coefficients on the order of 10%. Note, however, that the same set of dividing surfaces were employed for each of the electronic structure methods, which should ameliorate to some extent the limitations in the dividing surfaces when making comparisons. The final rate predictions include dynamical corrections of 0.9 and 0.85 for H atom additions and polyatomic additions, respectively. These dynamical corrections are based on our direct dynamics simulations for H + radical reactions[46] and for CH_3 + CH_3,[47] respectively.

The collisionless limit rate coefficients for H + HCO and for CH_3 + HCO are obtained from the steady state solution to the kinetics as described in ref. 48. This approach involves a matrix inversion of the rate coefficient matrix for given E and J followed by Boltzmann averaging. With this approach E and J are properly conserved and any rotational switching effects are correctly treated.

3. Results and discussion

3.1 H + CH_3 → CH_4

Radical–radical combination reactions present a special challenge to theory and H + CH_3 has been something of a benchmark for this class of reactions.[49–58] These reactions typically have no barriers and hence the dynamical bottlenecks for these reactions usually occur at large, 2–4 Å, separations between the two radical centers. It is well known that Hartree–Fock wavefunctions are poorly suited to this task. The problem here is that a restricted, Hartree–Fock wavefunction introduces spurious ionic character at large radical–radical separations and an unrestricted, Hartree–Fock wavefunction introduces significant spin contamination. In Fig. 1 we compare the full-CI potential curve of Dutta *et al.*[59] to RHF, UHF, RMP2, UMP2, RCCSD(T), UCCSD(T), RQCISD(T) and UQCISD(T) potential curves, all calculated with the same geometries and same basis set (6-31G*) used in the full-CI calculations. From this plot it can be seen that the RMP2, RCCSD(T) and RQCISD(T) all introduce artifactual, long-range barriers to the combination reaction. UMP2, UCCSD(T), and UQCISD(T), while not having barriers, are significantly less attractive than the full-CI potential in the critical 2–3 Å range. For example at a distance of 3 Å the UMP2, UCCSD(T), UQCISD(T) and full-CI binding energies are 0.8, 1.2, 1.2 and 2.8 kcal mol^{-1}, respectively. Thus the UMP2 interaction energy is in error by more than a factor of three while both UCCSD(T) and UQCISD(T) are in error by more than a factor of two.

A standard check on the quality of single-reference correlation methods can be made through the use of the T_1-diagnostic of Lee and Taylor.[60] The T_1 diagnostic is the Euclidean norm of the t_1 vector of the coupled-cluster wavefunction. It has been suggested that a T_1 diagnostic greater than 0.02 indicates

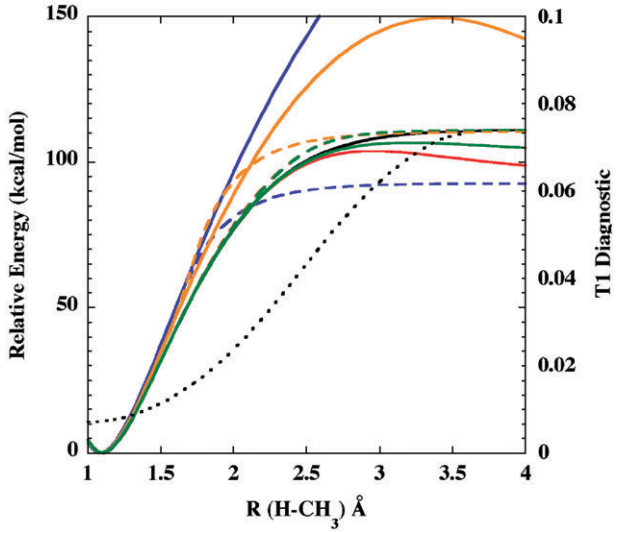

Fig. 1 Potential curves for H + CH_3 → CH_4. The full-CI potential curve (solid black) is from ref. 59. The other potential curves use the same basis set and geometries. All curves are shifted such that E_{min} = 0.0 kcal mol^{-1}. Solid lines denote restricted calculations, dotted lines denote unrestricted calculations. The color code is as follows: blue: Hartree–Fock; orange: MP2; red: CCSD(T), green: QCISD(T). The UCCSD(T) and UQCISD(T) curves are superimposed on this scale. Also shown is the T1 diagnostic (dotted black).

the need for a multi-reference wavefunction. In Fig. 1 we also show a plot of the T_1 diagnostic. It can be seen that the T_1 diagnostic becomes greater than 0.02 for R_{CH} > 1.9 Å, close to where the CCSD(T) and QCISD(T) calculations start to diverge significantly from the full-CI potential curve.

In Fig. 2 we compare multi-reference based potential curves to the same full-CI potential curve of Dutta *et al.*[59] The reference space for these calculations is a two electron, two orbital, complete active space (a total of 3 configurations). Note the scale here is 15 times smaller than that of Fig. 1. From this plot it is clear that CASPT2 and CAS + 1 + 2 + QC both adequately reproduce the full-CI potential curve even with this very small reference wavefunction. The CASSCF potential curve however is noticeably less attractive due to the neglect of dynamical correlation effects.

In Fig. 3 we compare spin un-restricted, DFT potential curves to the full-CI result. (Spin restricted DFT curves suffer from the same problems as the RHF, RMP2, RCCSD(T) and RQCISD(T) curves.) Here the question of basis sets is not as straightforward because DFT methods have been optimized to reproduce certain experimental data and thus are not expected to reproduce a small basis set full-CI result. In Fig. 3 we show four B3LYP curves, one using the same basis set, 6-31G*, used in the full-CI calculation and three using the larger Dunning basis sets, aug-cc-pVDZ, aug-cc-pVTZ and aug-cc-pVQZ. The MPW1K method is optimized to reproduce the kinetics of a series of abstraction reactions using a particular basis set, 6-31 + G**. The MPW1K results shown in Fig. 3 employ this same basis set. In addition to the full-CI/6-31G* curve we also show CASPT2 curves using the same four basis sets noted above for B3LYP. Given the excellent agreement between CASPT2, CAS + 1 + 2 + QC and full-CI demonstrated in

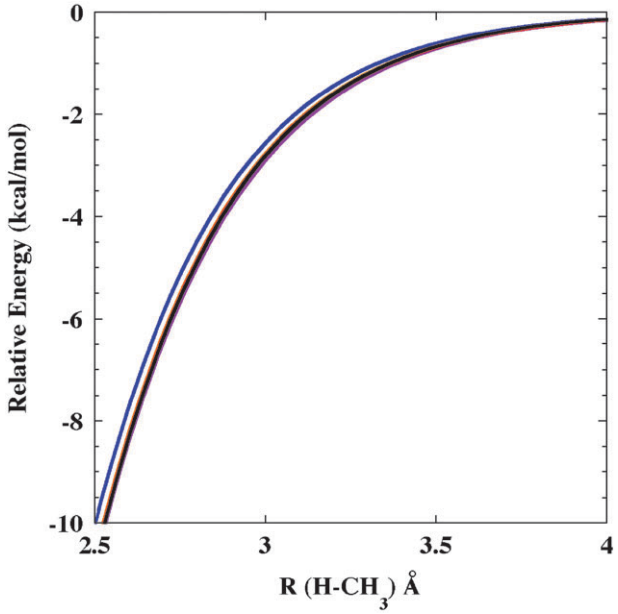

Fig. 2 Potential curves for H + CH_3 → CH_4. The full-CI potential curve (black) is from ref. 59. The other potential curves use the same basis set and geometries. All curves are shifted such that E(4.6 Å) = 0.0 kcal mol^{-1}. The color code is as follows: blue: CASSCF; purple: CASPT2; red: CAS + 1 + 2 + QC. Note the CASPT2, CAS + 1 + 2 + QC and FCI potential curves are all essentially superimposed on this scale.

Fig. 2 and the good agreement between the CASPT2/aug-cc-pVDZ, aug-cc-pVTZ and aug-cc-pVQZ curves, we believe these, large basis set, CASPT2 curves are a reasonable

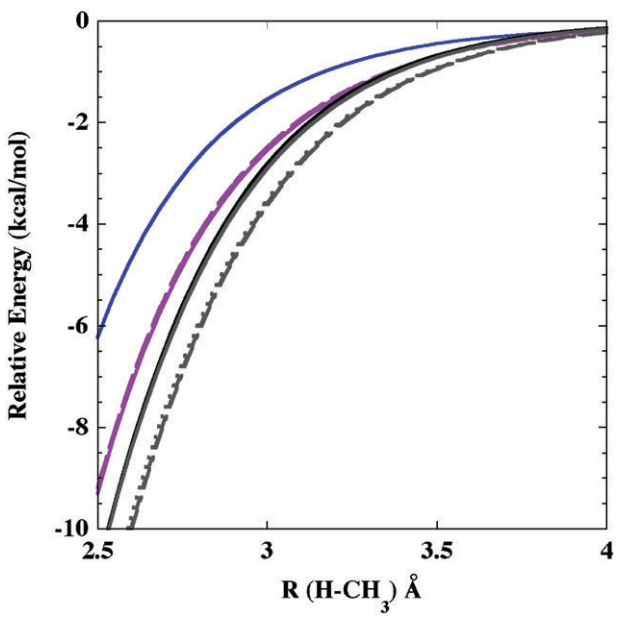

Fig. 3 Potential curves for H + CH_3 → CH_4. The full-CI potential curve (black) is from ref. 59. The other potential curves use the same geometries. All curves are shifted such that E(4.6 Å) = 0.0 kcal mol^{-1}. The key is as follows: blue, MPW1K; purple, B3LYP; gray, CASPT2; black, FCI. Basis set key for B3LYP and CASPT2: solid line, 6-31G*; dotted, aug-cc-pvdz; dashed, aug-cc-pvtz; dashed-dot, aug-cc-pvqz.

This journal is © the Owner Societies 2007

surrogate for an "experimental" potential curve and thus may be a more appropriate comparison for the DFT calculation's. Note that all of the Dunning basis set CASPT2 curves are nearly degenerate and are significantly more attractive than the CASPT2/6-31G* curve. This is an indication that the 6-31G* basis set is inadequate for the task of predicting the kinetics of this reaction.

From Fig. 3 we see the B3LYP/6-31G* potential curve is in reasonable agreement with the full-CI/6-31G* curve, better in fact than any of the single-reference, *ab initio* methods shown in Fig. 1. However, the B3LYP curve is found to be nearly independent of basis set with 6-31G*, aug-cc-pVDZ, aug-cc-pVTZ and aug-cc-pVQZ basis sets all giving essentially identical curves. At 3 Å the B3LYP interaction energy is ~30% less than that from the most accurate calculation. The agreement between the MPW1K and full-CI curves is poor and the comparison to the "experimental" curve is worse. At 3 Å the MPW1K interaction energy is ~60% less than that of the most accurate calculation.

In Fig. 4 we compare rate coefficients calculated with UMP2, UCCSD(T), CASSCF, CASPT2, B3LYP, and MPW1K. All of these calculations except MPW1K employ the aug-cc-pVDZ basis set. Use of a larger basis set for this reaction has little effect on the calculated rates. All of the calculated rates are multiplied by a temperature independent, dynamical correction of 0.9 to correct for re-crossing of the transition state dividing surface.[58] Also shown in Fig. 4 are experimental measurements of the rate.[61–63] The CASPT2 and B3LYP calculations both give rates that are in good agreement with the observed rates. The other calculations all give rates noticeably, but not greatly, lower. Overall then the conclusion from Fig. 4 is that for this reaction, all of these methods (with the exception of MP2) give rates that are within a factor of two of each other and experiment. This is not a general conclusion concerning radical–radical combination reactions as will be seen in the next section.

The CASPT2, CASSCF and B3LYP rates have essentially parallel positive temperature dependences while the MPW1K, CCSD(T) and MP2 all yield rates with noticeably less temperature dependence. At the lowest temperatures the CCSD(T) and MP2 rates start to curve up. At these lowest temperatures the transition state region is located at very large distances where the interaction potential will start to be dominated by dispersion forces. CASPT2, MP2 and CCSD(T) are all expected to treat dispersion interactions in a qualitatively correct fashion.

3.2 $CH_3 + CH_3 \rightarrow C_2H_6$

The $CH_3 + CH_3$ combination reaction has also been something of a benchmark for radical–radical combinations. We include it here to illustrate the differences between $H + CH_3$ and $CH_3 + CH_3$ caused by having two polyatomic radical reactants. There have been several *ab initio* studies of the potential surface for this reaction.[47,64–68] Potential curves for this reaction are shown in Fig. 5. The CASPT2 and CAS + 1 + 2 + QC calculations again employ a two electron, two orbital active space.

It is important to distinguish here between those methods which include dispersion interactions, namely CASPT2, CAS + 1 + 2 + QC, MP2, CCSD(T) and QCISD(T) and those that do not include dispersion interactions, B3LYP, MPW1K and CASSCF. The first group all yield similar long-range interaction potentials (see inset), all significantly more attractive than the second group. At shorter distances, where spin contamination effects start to become important the CASPT2

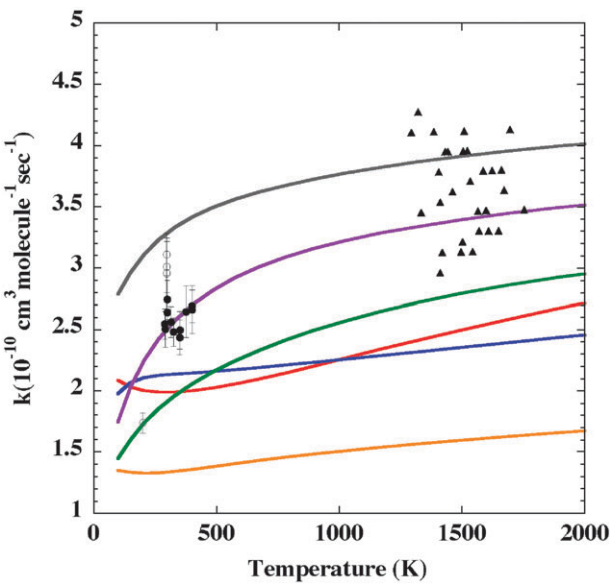

Fig. 4 High pressure limit rate coefficients for $H + CH_3 \rightarrow CH_4$. The color key is as follows: gray, CASPT2; green, CASSCF; purple, B3LYP; blue, MPW1K; red, CCSD(T); orange, MP2. The black symbols represent experimental results: solid circles are from ref. 61; open circles from ref. 62; and triangles from ref. 63.

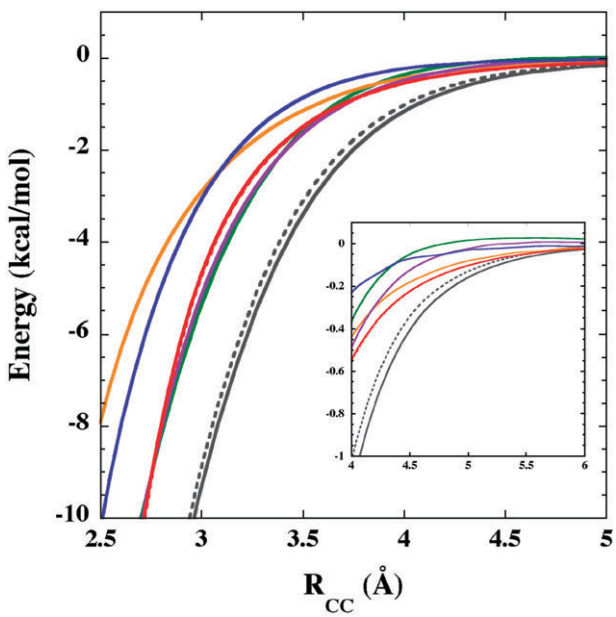

Fig. 5 Potential curves for $CH_3 + CH_3 \rightarrow C_2H_6$. The color key is as follows: solid gray, CASPT2; dashed gray, CAS + 1 + 2 + QC; green, CASSCF; purple, B3LYP; blue, MPW1K; solid red, CCSD(T); dashed red, QCISD(T); orange, MP2.

and CAS + 1 + 2 + QC curves become significantly more attractive than any of the others. Note that spin contamination of course still exists even at the longest distances but it does not affect the long-range behavior of the potential curves because the singlet and triplet surfaces become asymptotically degenerate.

In Fig. 6 we show high pressure rate coefficients obtained using five of the electronic structure methods from Fig. 5 along with the three highest-pressure experimental results available.[69–71] The agreement between experiment and the CASPT2 derived rate coefficients is excellent. The small differences at the higher temperatures are likely due to fall-off in the experimental results. The other methods give rate coefficients that are lower by factors ranging from about four (B3LYP) to over ten (MPW1K). This largely explains the low combination rate obtained by Lorant *et al.*[72] using B3LYP and more approximate partition function evaluation procedures. Note that while at high temperatures the MP2 rate coefficient is a factor of twenty below the CASPT2 rate this difference becomes much smaller at lower temperatures as the location of the transition state moves out to larger distances and starts to be dominated by dispersion interactions.

3.3 H + HCCH → C_2H_3

There have been at least four major theoretical studies of the H + HCCH → C_2H_3 reaction.[73–76] A summary of some of the calculated energetics from the various methods used in these studies is given in Table 1. The best available experimental estimate of the reaction exothermicity is −33.5 ±0.9 kcal mol^{-1}.[77] Most of the high-level *ab initio* calculations are in good agreement with this experimental estimate. The only outlier is the (5e,5o)-CASPT2 result. The CASPT2 calculations appear to be more sensitive to the size of the active space than the CAS + 1 + 2 + QC calculations. This does not appear to be a general conclusion as we and others[78] have found reactions for which CASPT2 is less sensitive to the size of the active space than CAS + 1 + 2 + QC. We also refer the reader to ref. 79 for a good discussion of issues related to CASPT2 active spaces.

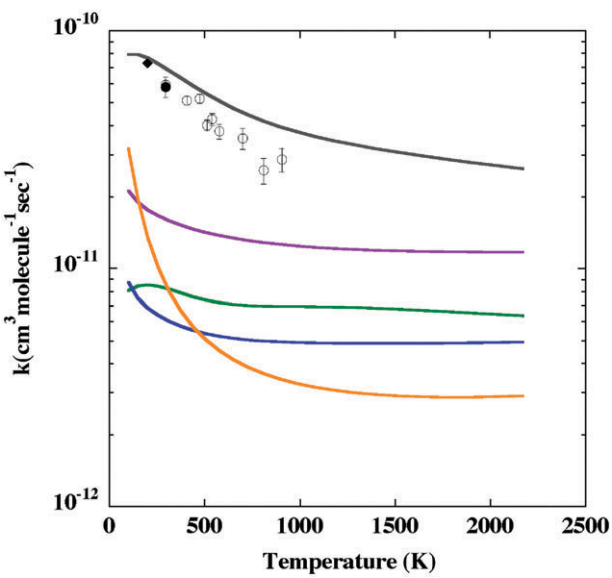

Fig. 6 High pressure limit rate coefficients for CH_3 + CH_3 → C_2H_6. The color key is as follows: gray, CASPT2; green, CASSCF; purple, B3LYP; blue, MPW1K; orange, MP2. The black symbols represent experimental results: the solid circle is from ref. 69, open circles from ref. 70 and the solid diamond from ref. 71. All of the theoretical rates have been multiplied by a dynamical (re-crossing) correction of 0.85 (see ref. 68).

Table 1 Relative energies (kcal mol^{-1}) for the reaction H + HCCH → C_2H_3. Energies are relative to the reactants. The numbers in parenthesis include zero point energies. The MP2, CCSD(T), QCISD(T), CASPT2 and CAS + 1 + 2 + QC calculations are all single point calculations using the aug-cc-pVQZ basis set at geometries determined using aug-cc-pVTZ basis sets

Methods	TS	C_2H_3
B3LYP/6-31 + G(d,p)	1.1(1.6)	−47.5(−41.4)
MPW1K	2.8(3.2)	−50.2(−44.0)
ROHF-RCCSD(T)	4.1(4.7)	−40.7(−34.4)
ROHF-UCCSD(T)	3.8(4.5)	−41.0(−34.6)
ROHF-RQCISD(T)	4.0(4.6)	−40.8(−34.5)
ROHF-UQCISD(T)	3.7(4.2)	−41.0(−34.7)
(3e,3o)-CAS + 1 + 2 + QC	4.3(4.8)	−40.1(−34.0)
(5e,5o)-CAS + 1 + 2 + QC	4.2(4.6)	−40.0(−33.9)
(3e,3o)-CASPT2	3.2(4.0)	−40.2(−33.6)
(5e,5o)-CASPT2	3.5(4.1)	−41.6(−35.2)
(11e,11o)-CASPT2	3.6(4.2)	−40.1(−33.9)

The CCSD(T), QCISD(T) and CAS + 1 + 2 + QC methods all give barrier heights in the range 3.7–4.2 kcal mol^{-1}, while the CASPT2 calculations give slightly lower barriers in the range 3.2–3.6 kcal mol^{-1} depending on the size of the active space. It appears that the CASPT2 barriers heights are trending upwards as the size of the active space is increased. Imposing spin restrictions on the CCSD(T) and QCISD(T) calculations raises the barrier heights by 0.3 kcal mol^{-1}. Note that the spin restriction also decreases the exothermicity of the reaction by 0.3 kcal mol^{-1} and thus has no effect of the barrier of the reverse reaction. The MPW1K barrier is a significant improvement over the B3LYP result but is still ∼1 kcal mol^{-1} below the more accurate CCSD(T), MRCI and CASPT2 results.

The transition state theory, high-pressure limit rates calculated using each of these methods are shown in Fig. 7. Also shown in Fig. 7 is the result of a direct measurement of the high-pressure limit rate using an H-maser, spin relaxation technique.[80,81] There have been many other measurements of the rate of this reaction, including temperature dependent studies, however, the H-maser study is the only one that directly measures the high-pressure limit. The TST rate based on the UQCISD(T) potential falls within the stated, ±5%, error bars of the experimental result. This level of agreement is fortuitous as it implies an accuracy of ±0.1 kcal mol^{-1} in the calculated barrier height whereas a more realistic estimate of the error bars expected from this level of theory would be ±0.5 kcal mol^{-1}. We conclude then that for this particular reaction all of the electronic structure methods used here are of comparable accuracy with the exception of the DFT methods.

Also shown in Fig. 7 are the results of two hybrid calculations in which geometries are determined using B3LYP/6-

This journal is © the Owner Societies 2007

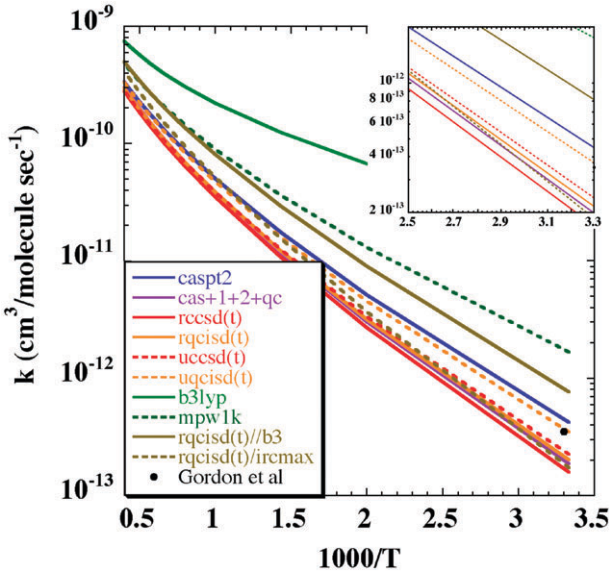

Fig. 7 High pressure limit rate coefficients for $H + C_2H_2 \rightarrow C_2H_3$. The experimental data point (black dot) is from ref. 80 and 81.

31 + G(d,p) followed by RQCISD(T) calculations at the B3LYP geometries. In one of these calculations the RQCISD(T) "transition state" energy is taken to be the energy at the B3LYP transition state geometry. In the second calculation, often termed IRCMAX,[82] a B3LYP reaction path is determined, RQCISD(T) calculations are then done along the B3LYP reaction path, and the RQCISD(T) "transition state" energy is taken to be the maximum along this 1-D path. From Fig. 6 it can be seen that the first of these two hybrid calculations gives a 300 K rate that is about 4 times that of the full RQCISD(T) rate while the IRCMAX calculation gives a rate that is low by only ~15%, again relative to the complete RQCISD(T) calculation.

Notably, all the methods except the DFT ones and the two hybrid ones converge as the temperature increases toward 2000 K. This convergence implies that the treatment of the TS frequencies with the CASPT2, CAS + 1 + 2 + QC, CCSD(T) and QCISD(T) methods are fairly consistent, while the B3LYP and MPW1K ones are not.

3.4 $H + HO_2 \rightarrow H_2 + O_2$

The reaction of hydroperoxyl radical with H atom to give molecular hydrogen and molecular oxygen proceeds *via* an early, low barrier and is exothermic by 55.3 ± 0.06 kcal mol^{-1}.[83] This reaction competes with the reactions $H + HO_2 \rightarrow 2OH$ and $H_2O + O$. The branching between these product channels has important consequences in atmospheric and flame chemistry. The reverse reaction is thought to be an important initiation mechanism in H_2/O_2 combustion. This system has been well studied experimentally,[84–88] and the potential energy surface has previously been characterized theoretically[89] using the QCISD(T) method and triple-zeta basis sets. The resulting transition state theory rate coefficients for $H + HO_2 \rightarrow H_2 + O_2$ were found to agree with available experimental results to within a factor of 3.5. More recently, the CCSD(T) method was used to compute the rate coefficient for the reverse reaction ($H_2 + O_2 \rightarrow H + HO_2$), and the results were found to be in excellent agreement with the accompanying high temperature experimental measurements.[86]

In Fig. 8, MP2, CASPT2 and MPW1K saddle points and IRC's for the triplet abstraction are shown as functions of the HH and OH bond distances. B3LYP/aug-cc-pvdz does not predict a saddle point for this reaction, and an IRC for this method was obtained by computing the steepest-descent path in mass-scaled coordinates from a partially optimized geometry in the entrance channel, where the H–H bond distance was constrained to 3.5 Å during the optimization of the starting point geometry. Density functional theory and MP2 are often used to optimize geometries and compute reaction paths, and Fig. 8 illustrates that these methods may predict significantly different saddle points and reaction paths (with bond distances differing by 0.1 Å or more). Furthermore, neither the MP2 nor the B3LYP result is in good agreement with the highest levels of theory considered here, *i.e.*, the ROHF-UCCSD(T) and ROHF-RQCCSD(T) saddle points, also shown in Fig. 8. The CASPT2 and MPW1K saddle points, in contrast, are in reasonable agreement with the high-level saddle points, and a similar accuracy may be expected for the corresponding IRC's.

In Table 2 we compare the energies of the three stationary points for this reaction using a variety of theoretical methods. The QCISD(T), CCSD(T), and CAS + 1 + 2 + QC calculations predict exothermicities for the reaction within 0.5 kcal mol^{-1} of the experimental result. The other methods, B3LYP, MPW1K, MP2 and CASPT2 are noticeably less accurate.

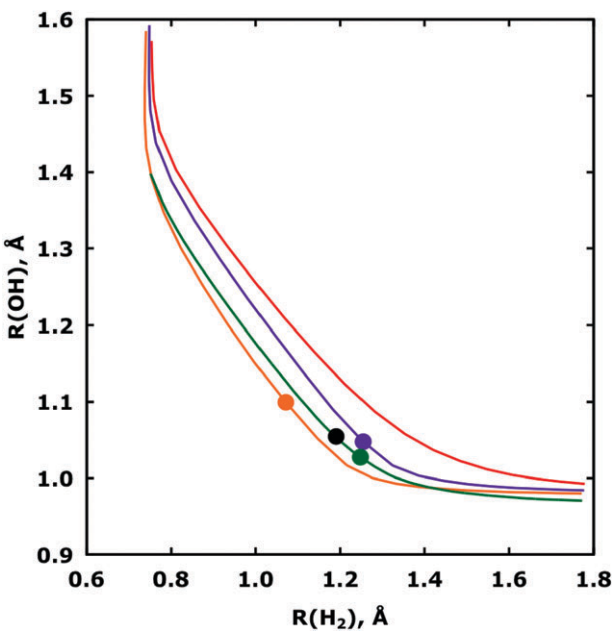

Fig. 8 Bond distances along the IRC for $H + HO_2 \rightarrow H_2 + O_2$, with saddle points indicated by dots. The color code is as follows: orange-MP2; red-B3LYP; green-MPW1K; purple-CASPT2. The ROHF-UCCSD(T) and ROHF-QCISD(T) saddle points (black) are superimposed.

Table 2 Relative energies (kcal mol^{-1}) for the H_2O_2 surface. Energies are relative to H + HO_2 (numbers in parenthesis include zero point energies). The MP2, CCSD(T), QCISD(T), CASPT2 and CAS + 1 + 2 + QC calculations are all single point calculations using the aug-cc-pVQZ basis set at geometries determined using aug-cc-pVDZ basis sets

Method	TS	H_2 + O_2
B3LYP/aug-cc-pVDZ	—	−53.8(−54.0)
MPW1K	1.6(0.5)	−52.6(−52.9)
UMP2	6.3(5.1)	−58.3(−58.8)
ROHF-RCCSD(T)	3.2(1.8)	−54.8(−55.1)
ROHF-UCCSD(T)	2.5(1.1)	−54.7(−55.1)
ROHF-RQCISD(T)	2.9(1.5)	−54.5(−54.8)
ROHF-UQCISD(T)	2.2(0.8)	−54.3(−54.6)
(14e,10o)-CAS + 1 + 2 + QC	2.6(1.4)	−55.2(−55.4)
(14e,10o)-CASPT2	1.6(0.3)	−58.3(−58.7)
Exp't		(−55.28 ± 0.06)

As with the H + HCCH reaction CCSD(T) barriers are slightly higher than QCISD(T) and spin restricted barriers are slightly higher than spin unrestricted but the differences are too small to make any judgment as to which are more accurate. The CASPT2 exothermicity differs from experiment and the high-level methods by 3–4 kcal mol^{-1}. The CASPT2 barrier height is also lower than the high level methods by ~1 kcal mol^{-1}. The multi-reference CI energies, using the same active space as in the CASPT2 calculation, agree very well with the CCSD(T) and QCISD(T) predictions.

A useful check on the convergence of the results with respect to the basis set can be made by doing calculations with two different basis sets and then extrapolating to a complete basis set (CBS) limit. One such extrapolation is given by the following formula[90]

$$E_{\text{aug-cc-pVxZ}} = E_{\text{CBS}} + \frac{B}{(n_x + 1)^4}$$

where $n_T = 3$ and $n_Q = 4$ for the aug-cc-pVTZ and aug-cc-pVQZ basis sets, respectively. For this reaction the aug-cc-pVQZ and aug-cc-pVTZ barrier heights differ by ~0.3 kcal mol^{-1} and the aug-cc-pVQZ barriers differ by less than 0.2 kcal mol^{-1} from the extrapolated CBS limits.

Fig. 9 shows electronic energies, relative to the HO_2 + H asymptote, along the IRC's from MPW1K, MP2, B3LYP, and CASPT2 calculations. None of these methods yield quantitative energies, and, as noted above, the forward barrier heights vary widely from 0–6.5 kcal mol^{-1}. Also shown are the ROHF-RQCISD(T)/CBS energies computed along each of these lower-level IRC's. The resulting ROHF-RQCISD(T) barrier heights vary from 3.0–4.3 kcal mol^{-1}. While this range of values is much smaller than the range of values predicted by the uncorrected lower level methods, errors of this magnitude in the barrier height will still be kinetically significant at low to moderate temperatures. The ROHF-RQCISD(T) maximum along the lower level IRC is shifted toward the products relative to the CASPT2 and MPW1K saddle points but toward the reactants relative to the MP2 saddle point.

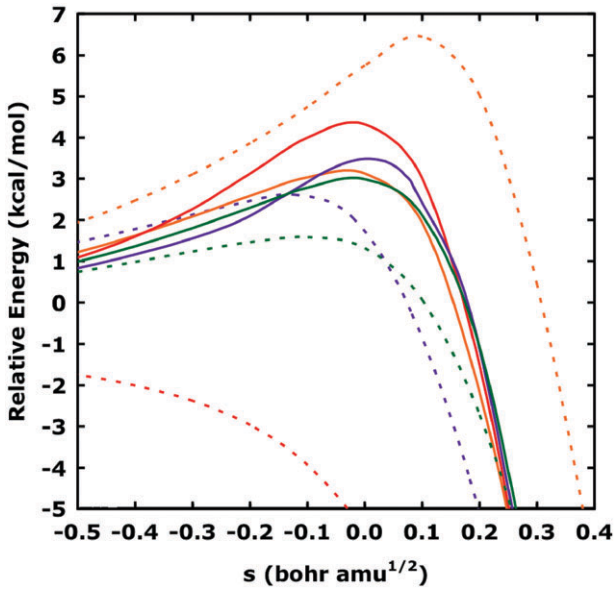

Fig. 9 Electronic energies along the IRC for H + HO_2 → H_2 + O_2. The color code is as follows: orange, MP2; red, B3LYP; green, MPW1K; purple, CASPT2. Dashed lines represent lower level energies, and solid lines represent ROHF-RQCISD(T)/CBS energies computed along the lower level reaction paths. The reaction coordinate s is set to zero at the maximum ROHF-RQCISD(T) energy for each lower level method.

The Q1 diagnostic is defined for the QCISD(T) method in a manner analogous to the T1 diagnostic for the CCSD(T) method. The Q1 diagnostics for the ROHF-RQCISD(T) calculations along all four IRC's vary from 0.04 in the reactant valley to 0.05–0.06 at the saddle point and 0.02–0.06 in the product valley. As discussed above for the T1 diagnostic, these values may indicate a need for multi-reference methods to accurately describe this system. However, the good agreement with the CAS + 1 + 2 + QC results argues against such problems.

SCT transmission coefficients were computed for the seven energy curves in Fig. 9 having barriers, and the results are plotted in Fig. 10. At low temperatures, κ was found to be extremely sensitive to the shape of the potential energy surface, varying from 1.4 to 55 for the low level methods and from 2.5 to 22 for the ROHF-RQCISD(T) energy curves at 300 K. At 1000 K, the range of κ values predicted by the high level methods is greatly decreased but still significant, increasing the rate by only 5–15% for the MP2, MPW1K, and CASPT2 IRC's and by more than 50% for the B3LYP IRC.

Rate coefficients were computed for the MP2, MPW1K, and CASPT2 potential energy surfaces and for the high level ROHF-RQCISD(T) energies computed along the MP2, B3LYP, MPW1K, and CASPT2 IRC's, and the results are shown in Fig. 11. In the high level calculations, the ROHF-RQCISD(T) energies were used to obtain barrier heights $V^{\dagger}$ and transmission coefficients κ, and low level frequencies and rotational constants (summarized in Table 3) were used to compute the partition functions $Q^{\dagger}$ and Q_R. Several previous experimental[84–88] and theoretical[86,89] results are also shown in Fig. 11, where the results of Michael *et al.*[86] for the reverse

 This journal is © the Owner Societies 2007

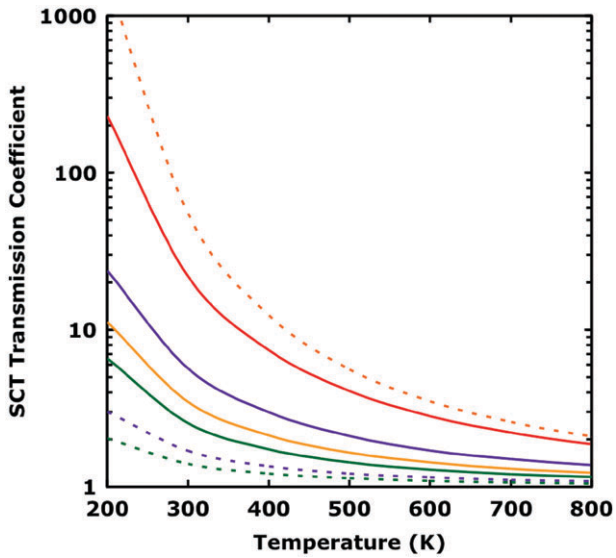

Fig. 10 Small curvature tunneling (SCT) transmission coefficients for $H + HO_2 \rightarrow H_2 + O_2$. The color code is as follows: orange, MP2; red, B3LYP; green, MPW1K; purple, CASPT2. Dashed lines represent uncorrected lower level results, and solid lines represent results for ROHF-RQCISD(T)/CBS energies computed along each of the lower level IRCs.

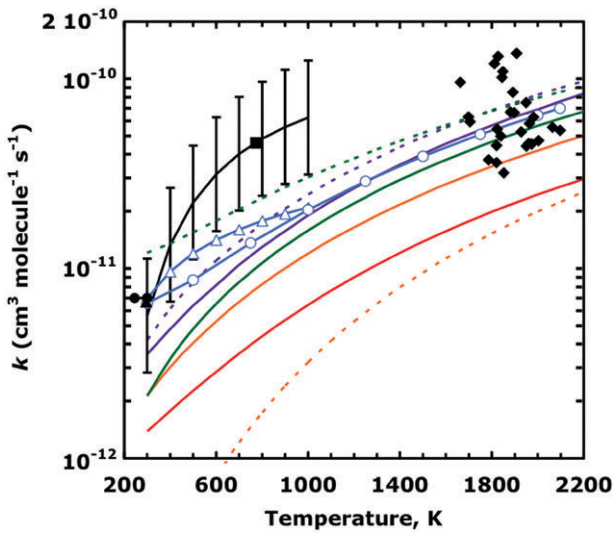

Fig. 11 Rate coefficient for $H + HO_2 \rightarrow H_2 + O_2$. The color code is as follows: orange, MP2; red, B3LYP; green, MPW1K; purple, CASPT2, with (solid) and without (dashed) high level ROHF-RQCISD(T)/CBS energy corrections. The recommended value of Baulch *et al.*[88] is shown as a black line. The previous theoretical results of Karkach and Osherov[89] (open triangles) and Michael *et al.*[86] (open circles) and experimental results of Baldwin and Walker[84] (filled square), Sridharan *et al.*[85] (filled triangle), Keyser[87] (filled circles), and Michael *et al.*[86] (filled diamonds).

reaction were transformed using the expression

$$K_{eq}(T) = 1.394(T/298\ \mathrm{K})^{0.3558} \exp(-27511\ \mathrm{K}/T),$$

which was fit to data obtained from the Active Thermochemical Tables.[91]

The CASPT2 rate coefficient and the ROHF-RQCISD(T) rate coefficient based on the CASPT2 IRC are in good agreement with one another and with room temperature and high temperature experimental results. This is perhaps surprising in light of the significantly different barrier heights for these two methods. The CASPT2 barrier height is 0.8 kcal mol^{-1} lower than the ROHF-RQCISD(T) barrier height along the CASPT2 IRC, and improving the barrier height alone would lead to a factor of 4 increase in the rate at 300 K and poor agreement with experiment. However, as seen in Fig. 10, the SCT tunneling correction for the CASPT2 IRC is one-third that of the ROHF-RQCISD(T) energy curve along the CASPT2 IRC, and the effects of errors in the barrier height and width largely cancel resulting in the good agreement between the two methods. This cancellation may be anticipated in general, as lowering the energy of the saddle point will typically result in a flatter potential curve near the barrier. However this also suggests that isotope effects calculated with these two methods might be dramatically different.

The ROHF-RQCISD(T) high level energy correction for the MP2 IRC improves the predicted rate coefficient dramatically, but is still a factor of two smaller than the results based on the CASPT2 IRC. The ROHF-RQCISD(T) rate coefficient computed for the B3LYP IRC is one-third that of the CASPT2 results. The high-level energy correction does not significantly improve the quality of the predicted rate coefficient for the MPW1K method, which was parameterized for kinetics, and both MPW1K rate coefficients are in good agreement with the experimental results. It is worth noting however that, with the exception of the calculations employing the MP2 and B3LYP IRC's, the range of the predicted rate coefficients is similar to the experimental uncertainty.

For the MPW1K and MP2 IRC's, significant cancellation is again observed in the effects of correcting the barrier heights and widths using high level energies, and, at temperatures above $\sim$500 K, the most significant effect on the predicted ROHF-RQCISD(T) rate coefficients arises from differences in the vibrational frequencies and rotational constants. As seen in Table 3, the product of the saddlepoint vibrational frequencies for the ROHF-QCISD(T) method differs from those of the CASPT2, MPW1K, MP2, and B3LYP methods by factors of 0.8, 1.6, 1.6, and 2.3, respectively, which correlates well with the relative rate coefficients predicted by the various methods at high temperatures.

3.5 $H_2CO \rightarrow$ products

Formaldehyde dissociation proceeds to two different sets of products *via* three distinct pathways, a molecular elimination path,

$$H_2CO \rightarrow H_2 + CO \tag{2}$$

via a "tight" transition state, a radical-forming dissociation path,

$$H_2CO \rightarrow H + HCO \tag{3}$$

and a third "roaming atom" path,

$$H_2CO \rightarrow H \cdots HCO \rightarrow H_2 + CO \tag{4}$$

Table 3 Vibrational frequencies and rotational constants (cm^{-1}) for the $H + HO_2 \rightarrow H_2 + O_2$ saddle point (SP) and HO_2[a]

Method		Frequencies	Rotational constants
MP2	SP	2684i, 380, 759, 1323, 1409, 1596	4.21, 1.01, 0.82
	HO_2	1199, 1451, 3654	20.4, 1.14, 1.08
B3LYP[b]	SP	554, 1002, 1128, 1310, 1468	4.04, 0.94, 0.77
	HO_2	1164, 1434, 3588	20.6, 1.13, 1.07
MPW1K	SP	1217i, 317, 653, 1288, 1486, 2075	4.04, 1.00, 0.80
	HO_2	1285, 1503, 3810	21.3, 1.17, 1.11
ROHF-RQCISD(T)	SP	1869i, 314, 665, 1145, 1362, 1621	3.98, 0.96, 0.77
	HO_2	1067, 1423, 3620	20.2, 1.09, 1.04
ROHF-UCCSD(T)	SP	1783i, 303, 654, 1138, 1362, 1689	3.97, 0.96, 0.77
	HO_2	1077, 1426, 3620	20.2, 1.09, 1.04
(14e,10o)-CASPT2	SP	1745i, 278, 617, 1106, 1353, 1732	3.90, 0.94, 0.76
	HO_2	1054, 1397, 3577	20.6, 1.13, 1.07
CCSD(T)[c]	SP	1825i, 321, 681, 1169, 1374, 1717	
	HO_2	1142, 1441, 3672	

[a] The 6-31+G(d,p) basis set is used for the MPW1K method, and the aug-cc-pVDZ basis set is used otherwise. [b] The B3LYP method does not predict a saddle point. Vibrational frequencies and rotational constants were determined at the maximum in the ROHF-RQCISD(T) energy along the IRC, and the imaginary frequency is not listed. [c] Ref. 86, cc-pVQZ basis set.

that leads to the molecular products *via* an internal, hydrogen abstraction.[92–96] In addition to these dissociation processes formaldehyde can also undergo an isomerization.

$$H_2CO \rightarrow HCOH \qquad (5)$$

The molecular elimination path, (2), is one of the most well studied reactions both experimentally[97–102] and theoretically.[103–114] It has also become a benchmark reaction for theoretical methods. Polik *et al.*[100] estimated a barrier for this reaction of 79.2 ± 0.8 kcal mol^{-1} by fitting the modified (tunneling corrected) transition state RRKM rate expression of Miller[115] to experimentally observed photo-dissociation decay rates (see also ref. 116). At the time, this appeared to be in good agreement with the best theoretical estimates. More recent calculations[114] however placed the barrier at 81.9 ± 0.3 kcal mol^{-1}, a result that has been shown[117] to be consistent with recent thermal rate measurements.[101,102] The cause of the ~3 kcal mol^{-1} difference between the barrier deduced from the photodissociation experiments and that derived from theory is unresolved, although it has been noted[114] that quantitative agreement can be achieved using a reactant density of states computed from an anharmonic force field rather than the observed state density.

The threshold for the radical dissociation path, (3), is 86.57 ± 0.16 kcal mol^{-1},[118] significantly higher than the barrier for reaction (2). However, because (−3) is barrierless, (3) has a larger pre-exponential factor than (2) and becomes the dominant process at high temperatures.

The "roaming atom" path has been well studied by Bowman and coworkers using trajectory calculations on an accurate, *ab initio* surface. Trajectories are found in which a CH bond is nearly broken, the hydrogen atom then orbits around the remaining HCO fragment, eventually abstracting the second hydrogen atom. Using PHOFEX spectroscopy, Suits and coworkers have observed that channel (4) has a threshold close to that for (3) and estimate that it contributes ~20% of the molecular products near threshold and more at higher energies.[96] We note that CASPT2 predicts the existence of a saddle point (possibly more than one) on the potential surface for this process. This saddle point, the structure of which is shown in Fig. 12, is predicted to lie only 0.1–0.2 kcal mol^{-1} below the H + HCO asymptote, has an imaginary frequency of 140 cm^{-1} and the two lowest bound frequencies are only 20 and 80 cm^{-1}. Because this pathway involves large amplitude, anharmonic motion, this saddle point (and the reaction path associated with it) should be regarded as only representative of the region of the potential surface controlling this process. A harmonic oscillator, rigid-rotor, transition state theory calculation based on this saddle point gives a high pressure limit dissociation rate at 1000 K approximately 20 times that of the tight transition state. An anharmonic treatment would likely give a much lower dissociation rate. The saddle point could not be located with the RCCSD(T) or RQCISD(T) methods.

Calculated energies for the stationary points for these reactions are summarized in Table 4. Here TS_T refers to the tight molecular dissociation transition state, TS_R refers to the roaming atom transition state, and TS_M refers to the isomerization transition state. The CCSD(T) and QCISD(T) results are in excellent agreement with each other and with experimental results where available. It should be noted that this excellent agreement between theory and experiment is partly fortuitous as corrections for non-perturbative triples, core-valence correlation, relativistic effects and anharmonicity can each be several tenths of a kcal mol^{-1}.

The multi-reference CASPT2 and CAS+1+2+QC calculations shown in Table 4 both employ an eight orbital, eight electron, active space consisting of all valence orbitals except the two, doubly-occupied, oxygen valence lone pairs. The CAS+1+2+QC energies (barrier and reaction

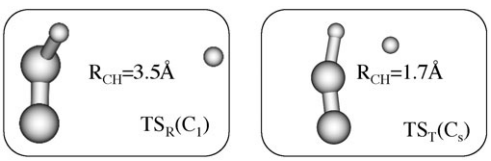

Fig. 12 CASPT2/aug-cc-pvdz geometries for the two transition states for the reaction, $H_2CO \rightarrow H_2 + CO$. TS_R is the roaming atom transition state. TS_T is the tight, molecular elimination saddle point.

This journal is © the Owner Societies 2007

Table 4 Relative energies (kcal mol^{-1}) for the H_2CO surface. Energies are relative to H_2CO (numbers in parentheses include zero point energies). The CCSD(T), QCISD(T) CAS + 1 + 2and CASPT2 calculations are all single point calculations using the aug-cc-pVQZ basis set at geometries determined using aug-cc-pVTZ basis sets. The CAS + 1 + 2 + QC calculations employ the CASPT2 geometries

Methods	H_2 + CO	H + HCO	Trans HCOH	TS_T	TS_R	TS_M
B3LYP						
6-31 + G(d,p)	9.8(2.6)	94.7(86.2)	52.4(52.4)	87.2(82.1)	94.3(85.9)	86.6(82.7)
aug-cc-pvdz	10.2(3.0)	92.3(83.9)	51.2(51.2)	83.9(78.9)	85.6(81.7)	92.3(83.9)
MPW1K	13.8(6.2)	94.3(85.5)	51.9(52.0)	93.9(88.6)	94.0(85.4)	89.4(85.4)
RCCSD(T)	5.1(−2.2)	95.0(86.4)	51.6(51.7)	86.6(81.2)	—	86.0(82.1)
RQCISD(T)	5.0(−2.3)	94.9(86.4)	51.6(51.7)	86.4(81.0)	—	85.8(81.8)
CAS + 1 + 2 + QC	4.4(−2.9)	94.4(86.0)	51.7(51.8)	85.9(80.5)	94.3(85.9)	85.8(81.9)
CASPT2	8.1(0.7)	94.1(85.7)	56.1(56.2)	87.1(81.8)	94.0(85.5)	88.7(84.9)
Exp't	(−2.2 ± 0.1)[a]	(86.57 ± 0.16)[c]		(79.2 ± 0.8)[d]		
	(−2.02 ± 0.05)[b]			(81.2 ± 0.9)[e]		

[a] D. L. Baulch, R. A. Cox, P. J. Crutzen, R. F. Hampson, Jr, J. A. Kerr, J. Troe and R. T. Watson, *J. Phys. Chem. Ref. Data* 1982, **11**, 327. [b] Ref. 91. [c] Ref. 118. [d] Ref. 100. [e] Ref. 117.

endothermicity) for reaction (5) are in nearly perfect agreement with the CCSD(T) and QCISD(T) energies. The CAS + 1 + 2 + QC energies for reactions (2) and (3) are systematically low by ~0.5 kcal mol^{-1} relative to the CCSD(T) and QCISD(T) energies. The disagreement between CASPT2 and CCSD(T) and QCISD(T) is significant. For example, the CASPT2 dissociation energy for reaction (2) is 3 kcal mol^{-1} higher, although the barrier height is only 0.5 kcal mol^{-1} higher. These energies are quite sensitive to the choice of active space. Inclusion of the oxygen valence lone pairs into the active space decreases the dissociation energy by 4 kcal mol^{-1} and the barrier height by 3 kcal mol^{-1} (see also the discussions in ref. 113 and 114).

The agreement between the B3LYP/6-31 + G(d,p) calculations and the high level *ab initio* methods is remarkably good, however this agreement deteriorates with the use of the larger aug-cc-pVDZ basis set. For these reactions the MPW1K energies are significantly less accurate than the B3LYP energies.

The high-pressure limit rates for reaction (2) are shown in Fig. 13. Unfortunately no high-pressure limit experiments are available for comparison. At 1000 K the ratios of the calculated rates, MPW1K : B3LYP : CAS + 1 + 2 + QC : QCISD(T) : CCSD(T) : CASPT2 are 0.03 : 4.1 : 1.9 : 1.5 : 1.3 : 1.0. The high level methods all give rates that are within a factor of two of each other while the MPW1K rate is much lower and the B3LYP rate is significantly higher. Most of the error in the DFT rates stems from errors in the barrier heights however there are also significant errors in the DFT frequencies (see Table 5). A crude estimate of the frequency contribution to the rate for a reaction such as this can be made by taking the ratio of the product of the frequencies of the reactant divided by the product of the frequencies of the transition state. The frequencies from the high level methods all give ratios within 1% of each other while the B3LYP ratio is low by 13% and the MPW1K ratio is low by 14%. For this reaction the DFT saddle point frequencies trend too high while the reactant frequencies trend too low. Thus for the B3LYP rate these errors in the frequencies partly cancel the error in the barrier height while for MPW1K the two errors add.

In Fig. 14 we show high-pressure limit rates for the reaction of H with HCO. There are two channels for this reaction, addition forming H_2CO, reaction (−3), and a direct abstraction to form H_2 + CO without going through the H_2CO well. All three methods shown predict the addition rate to be faster than the abstraction rate although the magnitude of the difference in rates varies considerably with B3LYP predicting the smallest difference and MPW1K the largest difference. As was the case for reaction (2), there are no high-pressure limit experiments for comparison. However, combining these results with the predictions for reaction (2) allows us to calculate zero pressure rates for the reaction,

$$H + HCO \rightarrow H_2 + CO \qquad (6)$$

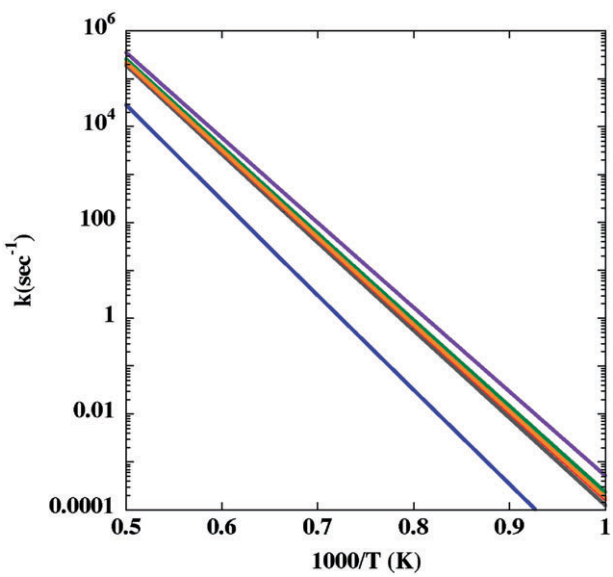

Fig. 13 High-pressure limit rate coefficients for $H_2CO \rightarrow H_2$ + CO using methods from Table 6. The color key is as follows: gray, CASPT2; green, CAS + 1 + 2 + QC; purple, B3LYP/aug-cc-pvdz; blue, MPW1K; orange, QCISD(T); red, CCSD(T).

Table 5 Vibrational frequencies (cm^{-1}) for H_2CO and the $H_2CO \rightarrow H_2 + CO$ saddle point (SP). The 6-31 + G(d,p) basis set is used for the MPW1K method, the aug-cc-pVDZ basis set is used for B3LYP and aug-cc-pVTZ for all of the higher-level methods

Method		Frequencies
MPW1K	SP	2026i, 832, 967, 1456, 2004, 3219
	H_2CO	1242, 1299, 1577, 1915, 3020, 3096
B3LYP	SP	1863i, 790, 898, 1338, 1899, 3152
	H_2CO	1194, 1246, 1513, 1803, 2891, 2959
QCISD(T)	SP	1830i, 782, 869, 1279, 1829, 3137
	H_2CO	1180, 1260, 1528, 1761, 2929, 2996
CCSD(T)	SP	1830i, 786, 869, 1282, 1837, 3140
	H_2CO	1180, 1260, 1528, 1764, 2930, 2998
CASPT2	SP	1765i, 781, 855, 1254, 1831, 3195
	H_2CO	1168, 1245, 1528, 1755, 2941, 2999

This reaction proceeds *via* two mechanisms, direct abstraction and addition/elimination. The addition/elimination path can further be broken into dissociation *via* the tight transition state for molecular elimination, reaction (2), and dissociation *via* the roaming atom mechanism, reaction (3). In our calculations we neglect the roaming atom mechanism which is expected to contribute ~5% to the rate of reaction (6). The results of these calculations are shown in Fig. 15 along with two low-pressure experimental measurements.[119,120] We also note that a recent trajectory study[121] of this reaction yielded a temperature independent rate in agreement with measurements of ref. 119. The CASPT2 and B3LYP calculations are in remarkably good agreement with each other and with the experimental results while the MPW1K rate is much lower due to its high barrier for molecular dissociation. The agreement between CASPT2 and B3LYP is partly fortuitous since, as noted above, the calculated rates of the two individual pathways differ by more than the difference in the final combined rates of reaction.

3.5 $CH_3CHO \rightarrow$ products

Acetaldehyde dissociation is similar to formaldehyde dissociation in that it proceeds to two different sets of products *via* three distinct pathways, a molecular elimination path,

$$CH_3CHO \rightarrow CH_4 + CO \quad (7)$$

via a "tight" transition state, a radical-forming dissociation path,

$$CH_3CHO \rightarrow CH_3 + HCO \quad (8)$$

and a third "roaming methyl" path,

$$CH_3CHO \rightarrow CH_3 \cdots HCO \rightarrow CH_4 + CO \quad (9)$$

that leads to the molecular products *via* an internal, hydrogen abstraction.[122] Calculations have previously been reported on the first two paths[123–128] but not the third. As was found in formaldehyde, a very loose transition state for the third, "roaming methyl", path can be found (with CASPT2). The geometries of the transition states for (7) and (9) are compared in Fig. 16. The energies of the relevant stationary points are given in Table 6. Here the multi-reference calculations employ an eight electron, seven orbital, active space (CCσ, CCσ*, COπ, COπ*, CHσ, CHσ*, On_p). The DFT results are similar to those for formaldehyde in that B3LYP/6-31 + G(d,p) gives

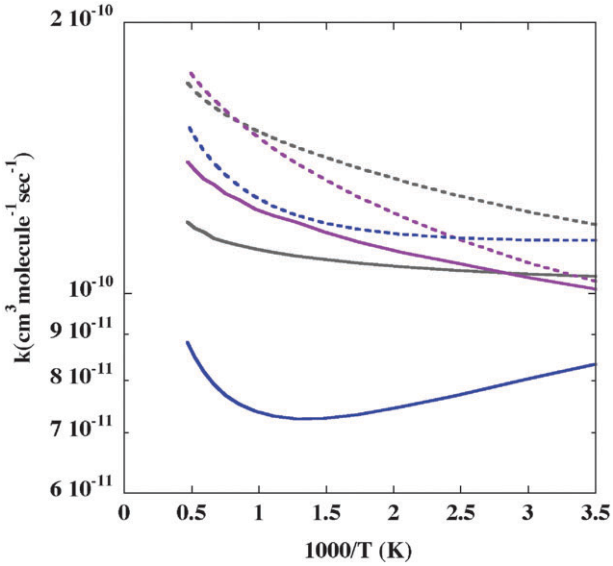

Fig. 14 High-pressure limit rate coefficients for H + HCO→ products. The color key is as follows: gray, CASPT2; purple, B3LYP/aug-cc-pvdz; blue, MPW1K. The solid curves are for the reaction H + HCO → H_2 + CO and the dashed curves for H + HCO → H_2CO.

an accurate prediction of the energy of the tight transition state but places the radical asymptote too low while MPW1K predicts the radical asymptote accurately but places the tight transition state much too high. The agreement between B3LYP and the higher-level calculations again deteriorates with the use of larger basis sets. About half of the ~1 kcal mol^{-1} error in the CC bond energy can be attributed to limitations of the aug-cc-pVTZ basis set. CASPT2/aug-cc-pVQZ calculations increase the bond energy by 0.5 kcal mol^{-1} but have no effect on the CH_3CHO-CH_4 + CO energy difference. The overall conclusion from the higher-level

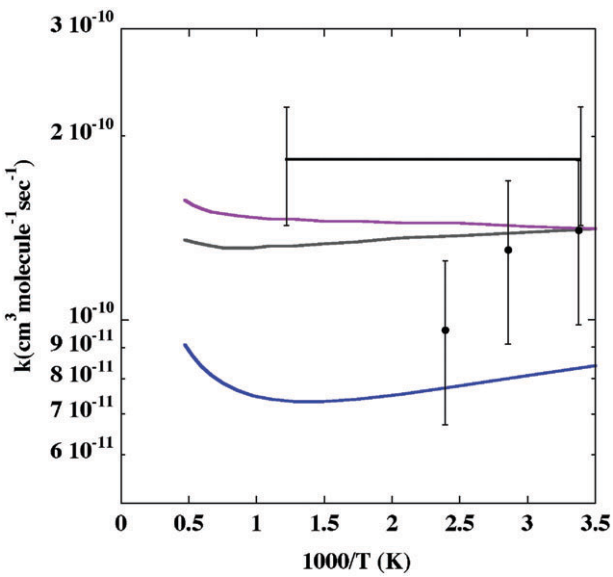

Fig. 15 Zero pressure rate coefficients for H + HCO → H_2 + CO The color key is as follows: gray, CASPT2; purple, B3LYP/aug-cc-pvdz; blue, MPW1K. Also shown are low pressure experimental results from ref. 119 (horizontal line) and 120 (solid circles).

This journal is © the Owner Societies 2007

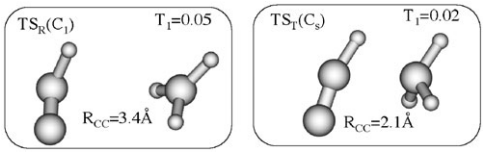

Fig. 16 CASPT2/aug-cc-pVDZ geometries for the two transition states for the reaction, $CH_3CHO \rightarrow CH_4 + CO$.

calculations in Table 6 is that the radical asymptote and the tight transition state are very close in energy both lying ~ 1 kcal mol^{-1} above the "roaming" transition state. In formaldehyde the "roaming" transition state is predicted to be only 0.1 kcal mol^{-1} below the radical asymptote. The larger stabilization of the "roaming" transition state relative to the radical asymptote in acetaldehyde can probably be attributed to long-range dispersion interactions.

The high-pressure limit rates for reaction (7) are shown in Fig. 17. Again no high-pressure limit experiments are available for comparison. At 1000 K the ratios of the calculated rates, MPW1K:B3LYP : CASPT2 : CAS + 1 + 2 + QC : QCISD(T) : CCSD(T) are 0.009 : 1.6 : 9.1 : 0.6 : 1.1 : 1.0. With the exception of CASPT2 all of the high level methods give rates within a factor of two of each other. The CASPT2 barrier is 4–5 kcal mol^{-1} lower than the other high-level methods and hence the CASPT2 rate is much higher. As for formaldehyde dissociation MPW1K predicts a barrier that is much too high and consequently a dissociation rate that is several orders of magnitude too low.

In Fig. 18 we show high-pressure limit rates for the reaction of CH_3 with HCO. There are two channels for this reaction, addition forming CH_3CHO, reaction (−8), and a direct abstraction to form CH_4 + CO without going through the CH_3CHO well. All three methods shown predict the addition and abstraction rates to be comparable at low temperature with the abstraction rate dropping more rapidly with increasing temperature. Unlike for H + HCO, both DFT methods predict CH_3 + HCO rates significantly slower than the CASPT2 result. This again is probably due to the lack of dispersion interactions in the DFT calculations. The results in Fig. 17 and 18 can be combined to give both high pressure and zero pressure rates for the reaction,

$$CH_3 + HCO \rightarrow \text{Products} \qquad (10)$$

As for H + HCO this reaction proceeds by both direct abstraction and addition/elimination mechanisms and we again neglect the contribution of the "roaming" methyl channel to addition/elimination. The calculated rates are shown in Fig. 19 along with previous experimental results[129–131] and the Tsang and Hampson[132] evaluation. The CASPT2 high-pressure limit is in essentially perfect agreement with the measurements of Baggot *et al.*[131] and Held *et al.*[129] The B3LYP and MPW1K rates are lower by factors of 3 and 5, respectively.

4. Conclusions

For problems where multi-reference effects are not important there is now a large body of evidence that CCSD(T) and QCISD(T) are capable of giving relative energies with high accuracy not only for stable species but also for transition states. This is true even for problems involving large changes in structure and bonding. Although multi-reference methods are also capable of yielding accurate relative energies for these kinds of problems, large changes in structure and bonding often require the use of large active spaces which can make the multi-reference calculations intractable. The real strength of multi-reference methods is for applications where single reference methods, such as CCSD(T) and QCISD(T), fail. Reaction (7) is a good example of a problem for which multi-reference methods are not particularly appropriate. The kinetics are controlled by a high barrier, involving large changes in the electronic structure relative to the reactant and an accurate multi-reference treatment would require a large

Table 6 Relative energies (kcal mol^{-1}) for the CH_3CHO surface. Energies are relative to CH_3CHO (numbers in parenthesis include zero point energies). The CCSD(T), QCISD(T) CAS + 1 + 2 + QC and CASPT2 calculations are all single point calculations using the aug-cc-pVTZ basis set at CASPT2/aug-cc-pVDZ geometries

Methods	CH_4 + CO	CH_3 + HCO	TS_T	TS_R
B3LYP				
6-31 + G(d,p)	1.1(−2.4)	86.3(78.5)	86.1(82.3)	85.9(78.5)
aug-cc-pVDZ	1.4(−2.2)	86.0(78.2)	84.9(80.9)	85.5(78.2)
aug-cc-PVTZ[a]	−0.7	85.0	84.1	85.1
MPW1K	5.5(1.7)	89.6(81.5)	94.4(90.3)	89.0(81.4)
RCCSD(T)	−2.9(−6.6)	89.6(81.9)	86.7(82.0)	84.8(77.0)
RQCISD(T)	−3.0(−6.7)	89.3(81.6)	86.5(81.7)	87.8(79.9)
CAS + 1 + 2 + QC	−0.5(−4.2)	88.1(80.4)	87.7(83.0)	87.2(79.3)
CASPT2	−3.7(−7.4)	85.4(77.8)	82.3(77.6)	84.4(76.5)
Exp't[b]	(−6.06 ± 0.1)	(82.8 ± 0.1)		

[a] Using B3LYP/aug-cc-pVDZ geometries. [b] Ref. 91.

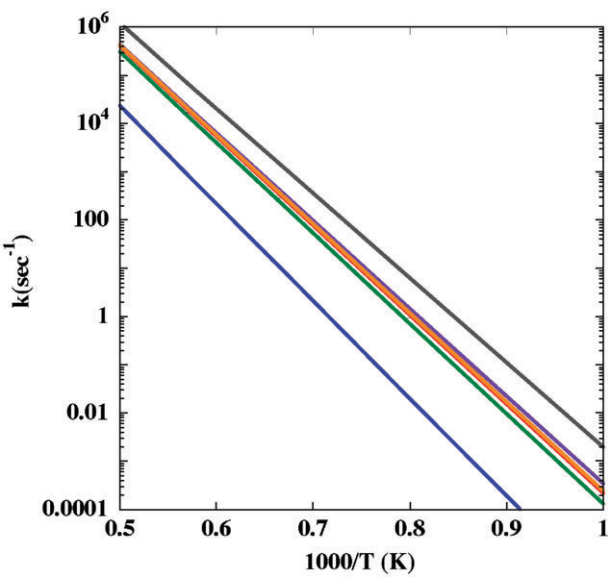

Fig. 17 High-pressure limit rate coefficients for $CH_3CHO \rightarrow CH_4$ + CO. Color code is the same as for Fig. 13.

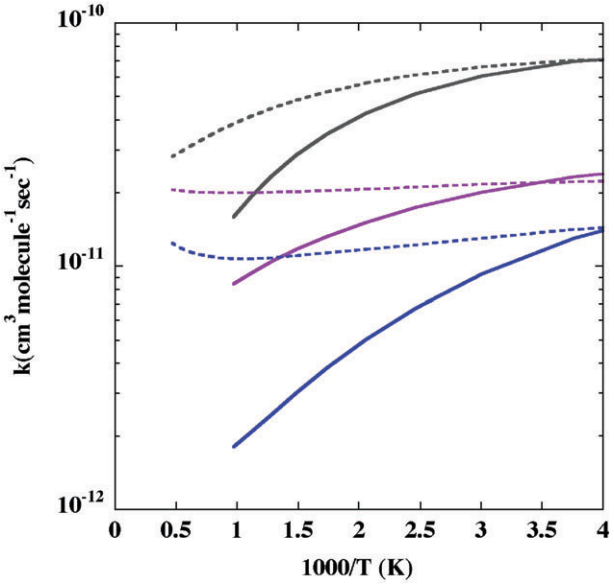

Fig. 18 High-pressure limit rate coefficients for CH_3 + HCO→ products. The color key is as for Fig. 14. The solid curves are for the reaction CH_3 + HCO → CH_4 + CO and the dashed curves for CH_3 + HCO → CH_3CHO.

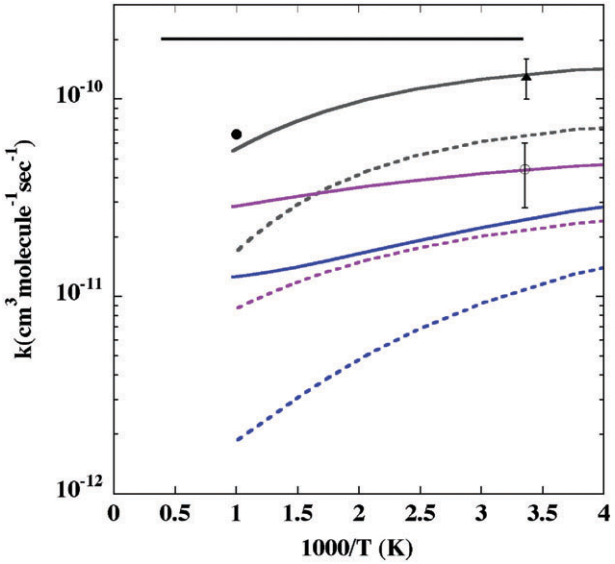

Fig. 19 High pressure and zero pressure rate coefficients for CH_3 + HCO → Products. High pressure results are solid lines. Zero pressure are dashed lines. The color key is as for Fig. 15. Also shown are experimental results as follows: solid circle, ref. 129; open circle, ref. 130; solid triangle, ref. 131; and horizontal black line, ref. 132.

active space (possibly full valence). However reaction (10), which actually involves the same transition state as (7) is a good example of where multi-reference methods are appropriate. Here the key features controlling the kinetics are the long-range, radical–radical interactions (for which single reference methods fail) and the height of the tight transition state relative to CH_3 + HCO (not relative to CH_3CHO). Although the CASPT2 calculation fails to accurately predict the barrier for (7) relative to CH_3CHO it does correctly predict the height of this barrier relative to CH_3 + HCO.

It is also interesting to compare CASPT2 and CAS + 1 + 2 + QC. As noted below CAS + 1 + 2 + QC is considerably more costly than CASPT2 but, at least for the reactions studied here, CAS + 1 + 2 + QC appears to give consistently more accurate results. However CASPT2 is closer to size consistent than CAS + 1 + 2 + QC and so as the size of the system increases one expects the accuracy of CAS + 1 + 2 + QC to degrade relative to CASPT2.

For the two DFT methods used here we find B3LYP to give more accurate results for radical–radical combinations, formaldehyde dissociation and acetaldehyde dissociation while MPW1K gives more accurate results for the H + HCCH addition and the H + HO_2 abstraction. In fact for radical–radical combinations, where multi-reference effects are important B3LYP is considerably more accurate than CCSD(T) and QCISD(T). For the relatively simple H + HCCH addition reaction neither DFT method gives results of kinetically useful accuracy, the room temperature MPW1K rate is high by almost an order of magnitude and the B3LYP rate is high by several orders of magnitude. One problem with the DFT methods is the neglect of dispersion interactions. This makes the DFT results much less accurate for reactions involving larger, polyatomic reactants. The DFT methods however do give qualitatively reasonable results for all the reactions considered here and are a very valuable tool for surveying complex potential surfaces.

Not yet discussed here is the question of relative cost of the *ab initio* methods. Taking as a representative problem, calculations on formaldehyde with the aug-cc-pVQZ basis set, the CPU times ratios for MP2 : CASPT2 : CCSD(T) : QCISD(T) : CAS + 1 + 2 + QC are approximately 1 : 2 : 4 : 4 : 12. The size scaling of these methods vary for different parameters such as the number of electrons, the number of occupied orbitals, the number of virtual orbitals, the size of the active space, *etc*. So, for example, the ratios for the calculations on acetaldehyde with the smaller aug-cc-pVTZ basis set are 1 : 3 : 22 : 22 : 13. Another issue that enters into the cost of calculations is the availability, or lack, of analytic derivatives (gradients and/or Hessians). Analytic gradients make efficient geometry optimizations and reaction path following possible. The MOLPRO package has analytic gradients for DFT methods and CASPT2. GAUSSIAN has analytic gradients and Hessians for DFT and MP2. Analytic gradients for multi-reference CI have been developed,[133–135] but not yet for the internally contracted CI.

The CASPT2 method provides more consistently accurate geometries than either of the DFT methods studied here and the CASPT2 frequencies are also in consistently better agreement with the QCISD(T) and CCSD(T) frequencies than are either of the two DFT methods. Thus, the CASPT2 approach is the preferred approach for obtaining geometries and frequencies in *a priori* kinetic studies.

Acknowledgements

This work is supported by the Division of Chemical Sciences, Geosciences, and Biosciences, the Office of Basic Energy

This journal is © the Owner Societies 2007

Sciences, the US Department of Energy, under DOE Contract Number DE-AC02-06CH11357.

References

1 T. H. Dunning, Jr, *J. Phys. Chem. A*, 2000, **104**, 9062.
2 T. H. Dunning, Jr, *J. Chem. Phys.*, 1989, **90**, 1007.
3 R. A. Kendall, T. H. Dunning, Jr and R. J. Harrison, *J. Chem. Phys.*, 1992, **96**, 6796.
4 F. B. Brown and D. G. Truhlar, *Chem. Phys. Lett.*, 1985, **117**, 307.
5 J. Villa, A. Gonzalez-Lafont, J. M. Lluch and D. G. Truhlar, *J. Am. Chem. Soc.*, 1998, **120**, 5559.
6 M. S. Gordon and D. G. Truhlar, *J. Am. Chem. Soc.*, 1986, **108**, 5412.
7 B. J. Lynch and D. G. Truhlar, *J. Phys. Chem. A*, 2003, **107**, 3898.
8 M. R. Nyden and G. A. Petersson, *J. Chem. Phys.*, 1981, **75**, 1843.
9 G. A. Petersson, A. Bennett, T. G. Tensfeldt, A. Al-Laham, W. A. Shirley and J. Mantzaris, *J. Chem. Phys.*, 1988, **89**, 2193.
10 G. A. Petersson and M. A. Al-Laham, *J. Chem. Phys.*, 1991, **94**, 6081.
11 G. A. Petersson, T. G. Tensfeldt and J. A. Montgomery, Jr, *J. Chem. Phys.*, 1991, **94**, 6091.
12 J. A. Montgomery, Jr, J. W. Ochterski and G. A. Petersson, *J. Chem. Phys.*, 1994, **101**, 5900.
13 J. W. Ochterski, G. A. Petersson and J. A. Montgomery, Jr, *J. Chem. Phys.*, 1996, **104**, 2598.
14 J. M. L. Martin, *Chem. Phys. Lett.*, 1996, **259**, 669.
15 P. L. Fast, L. Sanchez and D. G. Truhlar, *J. Chem. Phys.*, 1999, **111**, 2921.
16 A. K. Wilson and T. H. Dunning, Jr, *J. Chem. Phys.*, 1997, **107**, 8718.
17 T. Helgaker, W. Klopper, H. Koch and J. Noga, *J. Chem. Phys.*, 1997, **106**, 9639.
18 A. Halkier, T. Helgaker, P. Jorgensen, W. Klopper, H. Koch, J. Olsen and A. K. Wilson, *Chem. Phys. Lett.*, 1998, **286**, 243.
19 K. Raghavachari, G. W. Trucks, J. A. Pople and M. Head-Gordon, *Chem. Phys. Lett.*, 1989, **157**, 479.
20 J. A. Pople, M. Head-Gordon and K. Raghavachari, *J. Chem. Phys.*, 1987, **87**, 5968.
21 K. Andersson, P. Å. Malmqvist, B. O. Roos, A. J. Sadlej and K. Wolinski, *J. Phys. Chem.*, 1990, **94**, 5483.
22 K. Andersson, P. Å. Malmqvist and B. O. Roos, *J. Chem. Phys.*, 1992, **96**, 1218.
23 M. J. Frisch, G. W. Trucks, H. B. Schlegel, G. E. Scuseria, M. A. Robb, J. R. Cheeseman, V. G. Zakrzewski, J. A. Montgomery, Jr, R. E. Stratmann, J. C. Burant, S. Dapprich, J. M. Millam, A. D. Daniels, K. N. Kudin, M. C. Strain, O. Farkas, J. Tomasi, V. Barone, M. Cossi, R. Cammi, B. Mennucci, C. Pomelli, C. Adamo, S. Clifford, J. Ochterski, G. A. Petersson, P. Y. Ayala, Q. Cui, K. Morokuma, D. K. Malick, A. D. Rabuck, K. Raghavachari, J. B. Foresman, J. Cioslowski, J. V. Ortiz, B. B. Stefanov, G. Liu, A. Liashenko, P. Piskorz, I. Komaromi, R. Gomperts, R. L. Martin, D. J. Fox, T. Keith, M. A. Al-Laham, C. Y. Peng, A. Nanayakkara, C. Gonzalez, M. Challacombe, P. M. W. Gill, B. Johnson, W. Chen, M. W. Wong, J. L. Andres, C. Gonzalez, M. Head-Gordon, E. S. Replogle and J. A. Pople, *(GAUSSIAN 98)*, Gaussian, Inc, Pittsburgh, PA, 1998.
24 MOLPRO is a package of *ab initio* programs written by Werner, H.-J. and Knowles, P. J. with contributions from J. Almlof, R. D. Amos, A. Berning, D. L. Cooper, M. J. O. Deegan, A. J. Dobbyn, F. Eckert, S. T. Elbert, C. Hampel, R. Lindh, A. W. Lloyd, W. Meyer, A. Nicklass, K. Peterson, R. Pitzer, A. J. Stone, P. R. Taylor, M. E. Mura, P. Pulay, M. Schutz, H. Stoll and T. Thorsteinsson. The majority of calculations reported here were done with Version 2006.1.
25 J. Zheng, Y. Zhao and D. G. Truhlar, *J. Chem. Theor. Comput.*, 2007, **3**, 569.
26 A. D. Becke, *J. Chem. Phys.*, 1993, **98**, 5648.
27 R. H. Hertwig and W. Koch, *Chem. Phys. Lett.*, 1997, **268**, 345.
28 B. J. Lynch, P. L. Fast, M. Harris and D. G. Truhlar, *J. Chem. Phys.*, 2000, **104**, 4811.
29 C. Hampel, K. Peterson and H.-J. Werner, *Chem. Phys. Lett.*, 1992, **190**, 1.
30 P. J. Knowles, C. Hampel and H.-J. Werner, *J. Chem. Phys.*, 1993, **99**, 5219.
31 H.-J. Werner, *Mol. Phys.*, 1996, **89**, 645.
32 P. Celani and H.-J. Werner, *J. Chem. Phys.*, 2000, **112**, 5546.
33 P. Celani and H.-J. Werner, *J. Chem. Phys.*, 2003, **119**, 5044.
34 H.-J. Werner and P. J. Knowles, *J. Chem. Phys.*, 1988, **89**, 5803.
35 P. J. Knowles and H.-J. Werner, *Chem. Phys. Lett.*, 1988, **145**, 514.
36 S. R. Langhoff and E. R. Davidson, *Int. J. Quantum Chem.*, 1974, **8**, 61.
37 D. W. Silver and E. R. Davidson, *Chem. Phys. Lett.*, 1978, **52**, 403.
38 (*a*) D.-H. Lu, T. N. Truong, V. S. Melissas, G. C. Lynch, Y.-P. Liu, B. C. Garrett, R. Steckler, A. D. Isaacson, S. N. Rai, G. Hancock, J. G. Lauderdale, T. Joseph and D. G. Truhlar, *Comput. Phys. Commun.*, 1992, **71**, 235; (*b*) Y.-P. Liu, G. C. Lynch, T. N. Truong, D.-H. Lu and D. G. Truhlar, *J. Am. Chem. Soc.*, 1993, **115**, 2408.
39 D. G. Truhlar, B. C. Garrett and S. J. Klippenstein, *J. Phys. Chem.*, 1996, **100**, 12771.
40 B. Kerkeni and D. C. Clary, *Phys. Chem. Chem. Phys.*, 2006, **8**, 917.
41 POLYRATE—version 9.4, J. C. Corchado, Y.-Y. Chuang, P. L. Fast, W.-P. Hu, Y.-P. Liu, G. C. Lynch, K. A. Nguyen, C. F. Jackels, A. Fernandez Ramos, B. A. Ellingson, B. J. Lynch, V. S. Melissas, J. Villà, I. Rossi, E. L. Coitiño, J. Pu, T. V. Albu, R. Steckler, B. C. Garrett, A. D. Isaacson and D. G. Truhlar, University of Minnesota, Minneapolis, 2005.
42 GAUSSRATE—version 9.4, J. C. Corchado, Y.-Y. Chuang, E. L. Coitiño and D. G. Truhlar, University of Minnesota, Minneapolis, 2006.
43 S. J. Klippenstein, *J. Chem. Phys.*, 1992, **96**, 367.
44 Y. Georgievskii and S. J. Klippenstein, *J. Chem. Phys.*, 2003, **118**, 5442.
45 Y. Georgievskii and S. J. Klippenstein, *J. Phys. Chem. A*, 2003, **107**, 9776.
46 L. B. Harding, Y. Georgievskii and S. J. Klippenstein, *J. Phys. Chem. A*, 2005, **109**, 4646.
47 S. J. Klippenstein, Y. Georgievskii and L. B. Harding, *Phys. Chem. Chem. Phys.*, 2006, **8**, 1133.
48 D. K. Hahn, S. J. Klippenstein and J. A. Miller, *Faraday Discuss.*, 2001, **119**, 207.
49 R. J. Duchovic, W. L. Hase, H. B. Schlegel, M. J. Frisch and K. Raghavachari, *Chem. Phys. Lett.*, 1982, **89**, 120.
50 D. M. Hirst, *Chem. Phys. Lett.*, 1985, **122**, 225.
51 W. L. Hase, S. L. Mondro, R. J. Duchovic and D. M. Hirst, *J. Am. Chem. Soc.*, 1987, **109**, 2916.
52 F. B. Brown and D. G. Truhlar, *Chem. Phys. Lett.*, 1985, **113**, 441.
53 H. B. Schlegel, *J. Chem. Phys.*, 1985, **84**, 4530.
54 S. D. Peyerimhoff, M. Lewerenz and M. Quack, *Chem. Phys. Lett.*, 1984, **109**, 563.
55 M. Lewerenz and M. Quack, *J. Chem. Phys.*, 1988, **88**, 5408.
56 H. Furue, J. F. Leblanc, P. D. Pacey and J. M. Whalen, *Chem. Phys.*, 1991, **154**, 425.
57 L. B. Harding, *Ber. Bunsen-Ges. Phys. Chem.*, 1997, **101**, 363.
58 S. J. Klippenstein, Y. Georgievskii and L. B. Harding, *Proc. Combust. Inst.*, 2002, **29**, 1229.
59 A. Dutta and C. D. Sherrill, *J. Chem. Phys.*, 2003, **118**, 1610.
60 T. J. Lee and P. R. Taylor, *Int. J. Quantum Chem.*, 1989, **S23**, 199.
61 M. Brouard, M. T. Macpherson and M. J. Pilling, *J. Chem. Phys.*, 1989, **93**, 4047.
62 P. W. Seakins, S. H. Robertson, M. J. Pilling, D. M. Wardlaw, F. L. Nesbitt, R. P. Thorn, W. A. Payne and L. J. Stief, *J. Phys. Chem. A*, 1997, **101**, 9974.
63 M.-C. Su and J. V. Michael, *Proc. Combust. Inst.*, 2002, **29**, 1219.
64 E. M. Evleth and E. Kassab, *Chem. Phys. Lett.*, 1986, **131**, 475.
65 K. V. Darvesh, R. J. Boyd and P. D. Pacey, *J. Phys. Chem.*, 1989, **93**, 4772.
66 S. H. Robertson, D. M. Wardlaw and D. M. Hirst, *J. Chem. Phys.*, 1993, **99**, 7748.
67 M. Naroznij, *J. Chem. Soc., Faraday Trans.*, 1998, **94**, 2531.

68 S. J. Klippenstein and L. B. Harding, *J. Phys. Chem. A*, 1999, **103**, 9388.
69 H. Hippler, K. Luther, A. R. Ravishankara and J. Troe, *Z. Phys. Chem., Neue Folge*, 1984, **142**, 1.
70 I. R. Slagle, D. Gutman, J. W. Davies and M. Pilling, *J. Phys. Chem.*, 1988, **92**, 2455.
71 D. Walter, H.-H. Grotheer, J. W. Davis, M. Pilling and A. F. Wagner, *Proc. Combust. Inst.*, 1990, **23**, 107.
72 F. Lorant, F. Behar and W. A. Goddard, III and Y. Tang, *J. Phys. Chem. A*, 2001, **105**, 7896.
73 L. B. Harding, A. F. Wagner, J. M. Bowman, G. C. Schatz and K. Christoffel, *J. Phys. Chem.*, 1982, **86**, 4312.
74 V. D. Knyazev and I. R. Slagle, *J. Phys. Chem.*, 1996, **100**, 16899.
75 J. V. Michael, M.-C. Su, J. W. Sutherland, L. B. Harding and A. F Wagner, *J. Phys. Chem. A*, 2003, **107**, 10533.
76 J. A. Miller and S. J. Klippenstein, *Phys. Chem. Chem. Phys.*, 2004, **6**, 1192.
77 J. Berkowitz, G. B. Ellison and D. Gutman, *J. Phys. Chem.*, 1994, **98**, 2744.
78 M. L. Abrams and C. D. Sherrill, *J. Phys. Chem. A*, 2003, **107**, 5611.
79 Z. Azizi, B. O. Roos and V. Veryazov, *Phys. Chem. Chem. Phys.*, 2006, **8**, 2727.
80 E. B. Gordon, A. P. Perminov, B. I. Ivanov, V. I. Matyushenko, A. N. Pnonmarev and V. L. Tal'roze, *Sov. Phys. JETP (Engl. Transl.)*, 1973, **36**, 212.
81 E. B. Gordon, B. I. Ivanov, A. P. Perminov and V. E. Balalaev, *Chem. Phys.*, 1978, **35**, 79.
82 D. K. Malick, G. A. Petersson and J. A. Montgomery, Jr, *J. Chem. Phys.*, 1998, **108**, 5074.
83 B. Ruscic, R. E. Pinzon, M. L. Morton, N. K. Srinivasan, M.-C. Su, J. W. Sutherland and J. V. Michael, *J. Phys. Chem. A*, 2006, **110**, 6592.
84 R. R. Baldwin and R. W. Walker, *J. Chem. Soc., Faraday Trans. 1*, 1979, **75**, 140.
85 U. C. Sridharan, L. X. Qiu and F. Kaufman, *J. Phys. Chem.*, 1982, **86**, 4569.
86 J. V. Michael, J. W. Sutherland, L. B. Harding and A. F. Wagner, *Proc. Combust. Inst.*, 2000, **28**, 1471.
87 L. F. Keyser, *J. Phys. Chem.*, 1986, **90**, 2994.
88 D. L. Baulch, C. T. Bowman, C. J. Cobos, R. A. Cox, T. Just, J. A. Kerr, M. J. Pilling, D. Stocker, J. Troe, W. Tsang, R. W. Walker and J. Warnatz, *J. Phys. Chem. Ref. Data*, 2005, **34**, 757.
89 S. P. Karkach and V. I. Osherov, *J. Chem. Phys.*, 1999, **110**, 11918.
90 J. M. L. Martin and O. Uzan, *Chem. Phys. Lett.*, 1998, **282**, 16.
91 B. Ruscic, private communication of unpublished data using ATcT v. 1.35 C(A)TN v. 1.063.
92 R. D. Van Zee, M. F. Foltz and C. B. Moore, *J. Chem. Phys.*, 1993, **99**, 1664.
93 D. Townsend, S. A. Lahankar, S. K. Lee, S. D. Chambreau, A. G. Suits, X. Zhang, J. Rheinecker, L. B. Harding and J. M. Bowman, *Science*, 2004, **306**, 1158.
94 X. Zhang, J. L. Rheinecker and J. M. Bowman, *J. Chem. Phys.*, 2005, **122**, 11431.
95 J. M. Bowman and X. Zhang, *Phys. Chem. Chem. Phys.*, 2006, **8**, 321.
96 S. A. Lahankar, S. D. Chambreau, X. Zhang, J. M. Bowman and A. G. Suits, *J. Chem. Phys.*, 2007, **126**, 044314.
97 B. A. Degraff and J. G. Calvert, *J. Am. Chem. Soc.*, 1967, **89**, 2247.
98 R. D. McQuigg and J. G. Calvert, *J. Am. Chem. Soc.*, 1969, **91**, 1590.
99 J. G. Calvert and J. N. Pitt, *Photochemistry*, Wiley, New York, 1966.
100 W. F. Polik, D. R. Guyer and C. B. Moore, *J. Chem. Phys.*, 1990, **92**, 3453.
101 G. Friedrichs, D. F. Davidson and R. K. Hanson, *Int. J. Chem. Kinet.*, 2004, **36**, 157.
102 V. Vasudevan, D. F. Davidson, R. K. Hanson, C. T. Bowman and D. M. Golden, *Proc. Combust. Inst.*, 2007, **31**, 175.
103 R. L. Jaffe, D. M. Hayes and K. Morokuma, *J. Chem. Phys.*, 1974, **60**, 5108.
104 R. L. Jaffe and K. Morokuma, *J. Chem. Phys.*, 1976, **64**, 4881.
105 J. D. Goddard and H. F. Schaefer III, *J. Chem. Phys.*, 1979, **70**, 5117.
106 L. B. Harding, H. B. Schelgel, R. Krishnan and J. A. Pople, *J. Phys. Chem.*, 1980, **84**, 3394.
107 J. D. Goddard, Y. Yamaguchi and H. F. Schaefer III, *J. Chem. Phys.*, 1981, **75**, 3459.
108 M. J. Frisch, R. Krishnan and J. A. Pople, *J. Phys. Chem.*, 1981, **85**, 1467.
109 M. Dupuis, W. A. Lester, Jr, B. H. Lengsfield III and B. Liu, *J. Chem. Phys.*, 1983, **79**, 6167.
110 M. J. Frisch, J. S. Binkley and H. F. Schaefer III, *J. Chem. Phys.*, 1984, **81**, 1882.
111 M. Urban, V. Kello, I. Cernusak, J. Noga and G. H. F. Dierksen, *Chem. Phys. Lett.*, 1987, **135**, 346.
112 G. E. Scuseria and H. F. Schaefer III, *J. Chem. Phys.*, 1989, **90**, 3629.
113 H. Nakano, K. Nakayama, K. Hirao and M. Dupuis, *J. Chem. Phys.*, 1997, **106**, 4912.
114 D. Feller, M. Dupuis and B. C. Garrett, *J. Chem. Phys.*, 2000, **113**, 218.
115 W. H. Miller, *J. Am. Chem. Soc.*, 1979, **101**, 6810.
116 R. Hernandez, W. H. Miller, C. B. Moore and W. F. Polik, *J. Chem. Phys.*, 1993, **99**, 950.
117 J. Troe, *J. Phys. Chem. A*, 2007, **111**, 3862.
118 M.-C. Chuang, M. F. Foltz and C. B. Moore, *J. Chem. Phys.*, 1987, **87**, 3855.
119 G. Friedrichs, J. T. Herbon, D. F. Davidson and R. K. Hanson, *Phys. Chem. Chem. Phys.*, 2002, **4**, 5778.
120 R. S. Timonen, E. Ratajczak and D. Gutman, *J. Phys. Chem.*, 1987, **91**, 692.
121 J. Troe and V. Ushakov, *J. Phys. Chem. A,* DOI: 10.1021/jp0674017.
122 P. L. Houstin and S. H. Kable, *Proc. Natl. Acad. Sci. U. S. A.*, 2006, **103**, 16079.
123 J. M. Martell, H. Yu and J. D. Goddard, *Mol. Phys.*, 1997, **92**, 497.
124 B. J. Smith, M. T. Nguyen, W. J. Bouma and L. Radom, *J. Am. Chem. Soc.*, 1991, **113**, 6452.
125 B. F. Gherman, R. A. Friesner, T.-H. Wong, Z. Min and R. Bersohn, *J. Chem. Phys.*, 2001, **114**, 6128.
126 Y. Kurosaki and K. Yokohama, *J. Phys. Chem. A*, 2002, **106**, 11415.
127 Y. Kurosaki, *Chem. Phys. Lett.*, 2006, **421**, 549.
128 K. S. Gupte, J. H. Kiefer, R. S. Tranter, S. J. Klippenstein and L. B. Harding, *Proc. Combust. Inst.*, 2007, **31**, 167.
129 A. M. Held, K. C. Manthorne, P. D. Pacey and H. P. Reinholdt, *Can. J. Chem.*, 1977, **55**, 4128.
130 S. A. Malenko, *Rev. Roum. Phys.*, 1987, **32**, 173.
131 J. E. Baggott, H. M. Frey, P. D. Lightfoot and R. Walsh, *J. Phys. Chem.*, 1987, **91**, 3386.
132 W. Tsang and R. F. Hampson, *J. Phys. Chem. Ref. Data*, 1986, **15**, 1087.
133 R. Shepard, in *Modern Electronic Structure Theory. Part I*, ed. D. R. Yarkony, World Scientific, Singaporem, 1995, p. 345.
134 H. Lischka, R. Shepard, R. M. Pitzer, I. Shavitt, M. Dallos, T. Muller, P. G. Szalay, M. Seth, G. S. Kedziora, S. Yabushita and Z. Zhang, *Phys. Chem. Chem. Phys.*, 2001, **3**, 664.
135 M. Dallos, T. Muller, H. Lischka and R. Shepard, *J. Chem. Phys.*, 2001, **114**, 746.

 This journal is © the Owner Societies 2007